Soil Dynamics and Earthquake Engineering

AGGRAVATION FACTORS FOR 2D SITE EFFECTS IN SEDIMENTARY BASINS: THE CASE OF NORCIA BASIN, CENTRAL ITALY

--Manuscript Draft--

Manuscript Number:	SOILDYN-D-20-00298
Article Type:	Research Paper
Keywords:	Aggravation factors - Basin effects - Earthquake - Wave propagation
Corresponding Author:	Ricardo Rodriguez-Plata, M.Sc IUSS: Scuola Universitaria Superiore Pavia pavia, pavia ITALY
First Author:	Ricardo Rodriguez-Plata, M.Sc
Order of Authors:	Ricardo Rodriguez-Plata, M.Sc
	A.G. Ozcebe
	C. Smerzini
	C.G. Lai
Abstract:	In this article the seismic site response in the Norcia basin, Central Italy, during the October 2016 M 6.5 earthquake, has been analyzed using both 1D and 2D ground response numerical models. Period-dependent aggravation factors (PDAFs) quantifying the difference between 2D and 1D site response are provided for two representative cross-sections of the basin. Time-domain linear visco-elastic and non-linear analyses were carried out with the finite difference commercial program FLAC2D. Although the basin sediments are constituted by rather stiff soils, the Norcia basin is found to produce a consistent modification and enhancement of ground motion. It is shown that the most important source of ground motion aggravation was the generation of Rayleigh waves at the basin edges. The variation of the PDAFs was explored by considering the effects of frequency content of input motion, damping ratio, irregularity of the alluvial-bedrock interface and the non-linear response of the sediments.
Suggested Reviewers:	Alessandro Pagliaroli Università degli Studi Gabriele d'Annunzio Chieti e Pescara - Sede di Pescara: Universita degli Studi Gabriele d'Annunzio Chieti Pescara - Sede di Pescara alessandro.pagliaroli@unich.it
	Lucia Luzi Istituto Nazionale di Geofisica e Vulcanologia Sezione di Milano lucia.luzi@ingv.it
	Kyriazis Pitilakis Aristotle University of Thessaloniki: Aristoteleio Panepistemio Thessalonikes pitilakis@civil.auth.gr
	Panjamani Anbazhagan Indian Institute of Science anbazhagan@iisc.ac.in

Powered by Editorial Manager® and ProduXion Manager® from Aries Systems Corporation

Highlights

- Modelling of 2D seismic wave propagation using finite differences
- Seismic site effects caused by basin edge generated surface waves in shallow basins
- Effect of soil nonlinear response on 2D aggravation factors in sedimentary basins

Manuscript File

AGGRAVATION FACTORS FOR 2D SITE EFFECTS IN SEDIMENTARY BASINS: THE CASE OF NORCIA BASIN, CENTRAL ITALY

Authors: R. Rodriguez-Plata[a,d,*], A.G. Ozcebe[a,b], C. Smerzini[a], C.G. Lai[b,c]

[a] Department of Civil and Environmental Engineering, Politecnico di Milano, P.za L. da Vinci 32, 20133 Milano, Italy

[b] Department of Civil and Architectural Engineering, University of Pavia, Via A. Ferrata, 3, 27100 Pavia, Italy

[c] European Centre for Training and Research in Earthquake Engineering (EUCENTRE), Via A. Ferrata, 1 27100 Pavia, Italy

[d] University School for Advanced Studies IUSS Pavia, Piazza della Vittoria 15, Pavia 27100, Italy

Corresponding author at IUSS Pavia, Italy :

ricardo.rodriguezplata@iusspavia.it (R. Rodriguez-Plata)

ABSTRACT**:** In this article the seismic site response in the Norcia basin, Central Italy, during the October 2016 M 6.5 earthquake, has been analyzed using both 1D and 2D ground response numerical models. Period-dependent aggravation factors (PDAFs) quantifying the difference between 2D and 1D site response are provided for two representative cross-sections of the basin. Time-domain linear visco-elastic and non-linear analyses were carried out with the finite difference commercial program FLAC2D. Although the basin sediments are constituted by rather stiff soils, the Norcia basin is found to produce a consistent modification and enhancement of ground motion. It is shown that the most important source of ground motion aggravation was the generation of Rayleigh waves at the basin edges. The variation of the PDAFs was explored by considering the effects of frequency content of input motion, damping ratio, irregularity of the alluvial-bedrock interface and the non-linear response of the sediments.

Keywords: Aggravation factors – Basin effects – Earthquake – Wave propagation

1.Introduction

It has been long recognized that strong ground motion and its spatial variability are strongly affected by the local geological conditions. The modification of ground motion characteristics by complex subsurface geology or by the presence of particularly soft sediments have been responsible for significant damage during past earthquakes. In particular, the presence of complex 2D or 3D geological structures – such as sedimentary basins - had been identified as responsible for the severity and uneven distribution of damage during strong earthquakes. A few examples are: the damage belt in Kobe during the Mw 7.2 1995 Hyogo-Ken Nambu earthquake (Kawase, 1996a); the damage observed in the Santa Monica area on the 17th of January 1994 during the Mw 6.7 Northridge earthquake (Graves et al., 1998); the collapse of buildings in the Armenian city of Kerikovan during the 1988 Ms 6.8 earthquake, which was attributed to local amplification generated by the city valley (Yegian, 1994); and the uneven damage distribution in the town of Skopje in North Macedonia during the MW 6.1 1963 earthquake (Poceski, 1969). Numerical studies and experimental sites such like the

Euroseistest (Raptakis et al., 2004) and the Rhone valley (Roten and Fäh, 2007) have also provided interesting insights about these site effects in 2D and 3D geological configurations.

In current advanced seismic building codes provisions, site effects are incorporated in the form of amplification factors which modify the amplitude and shape of the design acceleration response spectrum defined for reference rock conditions. Such factors are intended to account for the one-dimensional amplification of ground motion, either estimated by 1D ground response analyses or obtained according to the site classification scheme adopted by the specific building code at hand. Therefore, site-effects assessment is based on the assumption that the geologic structure, beneath the site under study, can be approximated by a stack of horizontally parallel layers overlying the bedrock. Also normal incidence is assumed for the angle of incidence of the upward traveling S waves. However, one-dimensional amplification is indeed inadequate to consider the complex wave propagation phenomena that takes place on 2D or even 3D geologic configurations such as cliffs, trenches or sedimentary basins. In such conditions, they may provide unsafe estimates, as they cannot take into account the buried morphological irregularities and lateral confinement of sedimentary basins. These features may be responsible for the generation of edge-induced surface waves which may further increase the amplitude and duration of ground motion in addition to reverberation phenomena and wave focusing.

An effective strategy to incorporate complex site effects into building codes is the implementation of *aggravation factors* on response spectral ordinates, which were first introduced by Chavez Garcia and Faccioli (2000) and examined in a number of recent studies (e.g. Riga et al., 2016; Zhu et al., 2016; Madiai et al., 2017). The term *aggravation factor* can be defined as the additional effect of 2D/3D site-amplification to be considered in addition to the standard *soil factor* used to account for 1D ground amplification. Quantitatively, 2D/3D aggravation factors are defined as the ratio between the ordinates of the acceleration response spectrum, as computed at the free surface of a basin from 2D/3D studies of ground amplification over the spectral accelerations calculated using an equivalent 1D site model. This ratio is referred hereinafter as Period Dependent Aggravation Factor (PDAF). Therefore, under the assumption that in seismic building codes seismic actions are defined in terms of spectral accelerations due to 1D site amplification, PDAFs can be used to correct design acceleration response spectra to account for the additional 2D/3D effects.

The present study addresses the evaluation of seismic response at the Norcia basin, a sedimentary valley located in Central Italy. This region is widely recognized for its high seismic hazard, having been hit by several strong earthquakes in the past 20 years, such as the Mw 5.8 Molise (October 31, 2002), the Mw 6.1 L'Aquila (April 6, 2009), the Mw 6.0 Amatrice (August 24, 2016), and the Mw 6.5 Norcia (October 30, 2016). The last two events were part of a long-lasting seismic sequence initiated in August 2016, which caused severe damage in the municipalities of Amatrice, and later in the town of Norcia. This sequence and its consequences have been the subject of important researches, focusing on the analysis of near-source ground motion and the seismic response of the intra-mountain valleys of the Central Apennines (e.g. Chiaraluce et al., 2017, Luzi et al., 2017).

As a contribution to the research of the ReLUIS RS2 project, funded by the Italian Department of Civil Protection, this work aims at quantifying the 2D site effects, if any, at the Norcia basin, in relation to estimates provided by 1D standard approaches for site response. This was achieved by estimating the PDAF spatial distribution obtained from 2D and 1D ground response analyses performed on two representative cross-sections of the basin. Normal incidence of plane SV waves was considered by making use of the finite difference commercial software FLAC 2D (Itasca, 2007). The

analyses were performed with particular reference to the October 2016 earthquake, hereinafter referred as 30-OCT.

In the next Section the description of Norcia basin is presented, along with the adopted seismo-stratigraphic model. Section 5 gives an introduction about the PDAFs, while Section 4 illustrates the assumptions under which the different types of analyses were performed. On Section 5, the 2D response of the cross sections under consideration is examined in both time and frequency domain. Finally, the results in terms of maximum PDAFs are presented and discussed in Section 6, whereas the conclusions are drawn in Section 7.

2. Geometrical and mechanical description of the Norcia basin.

The Norcia basin is a quaternary tectonic depression located in Central Italy, formed during the Apennines chain uplift (Galadini et al., 2003). It is approximately 10 km long and 3 km wide and it is mainly composed by two different Pleistocene to Holocene fluvial-lacustrine structures. The tectonic evolution of the basin has been dominated by the activity of a normal fault system located closed to its Northeast border. This system is composed by Norcia, Campi and Preci faults and belongs to the parallel active normal faulting sets of the central Apennines (Galli et al., 2005).

As presented by Özcebe et al. (2019), the geometry and shear wave velocity distribution of the sediment cover were estimated by combining the available geological information with additional geophysical and gravimetric data. As a result, the contour map representing the sediment-bedrock interface depth is presented on the left panel of Figure 1. The shear wave velocity distribution with depth, $V_S(z)$, is given Eq. (1). This function is graphically compared with the available measured V_S profiles on the right panel of Figure 1. A constant value of 0.4 is used for the Poisson ratio of the sediments. Note that the Norcia sediments are rather stiff with Vs_{30} ~= 500m/s, corresponding to EC8 site class B.

$$V_s(z)=Vs_{min}+\frac{2(Vs_{ref}-Vs_{min})}{1+\left(\frac{z_{ref}}{z}\right)^n} \qquad (1)$$

where Vs_{min} = 282 m/s; Vs_{ref} = 548 m/s; z_{ref} = 15 m; n= 1.29; z = depth in meters.

Similarly, for the sediments density (in ton/m^3):

$$\rho_{(z)} = 1.9 + \frac{0.6\,z}{400} \qquad (2)$$

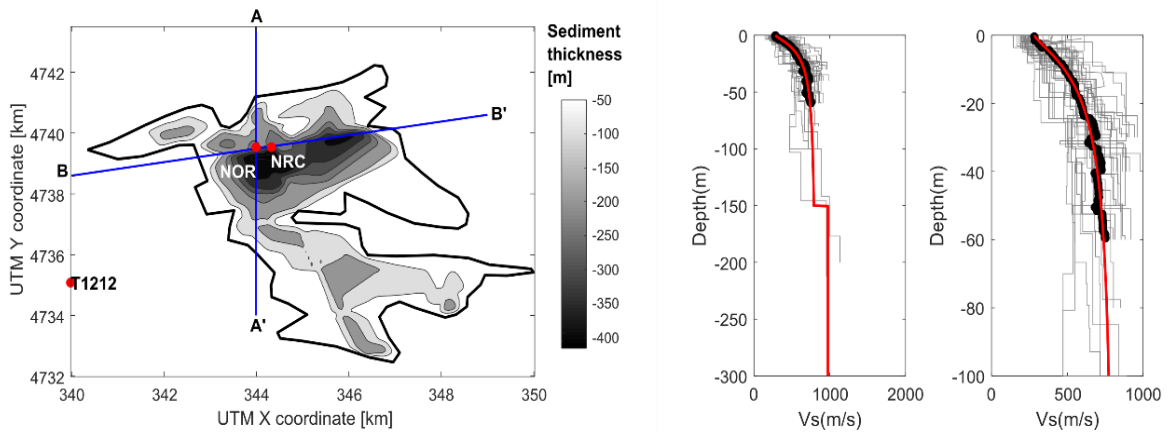

Figure 1. Depth-velocity model adopted for the Norcia basin (from Özcebe et al., 2019). Left, spatial distribution of sediment thickness. Left, comparison of the basin velocity model with the available field data (measured V_S-depth relation: gray lines, averages: black dots, velocity model: red line).

The contour map shown in Figure 1 also depicts the location of the two cross-sections selected for the 2D ground response analyses as well as the position of three available accelerometric stations whose recorded motions were used to calibrate the input parameters of the numerical models adopted to carry out 1D and 2D ground response analyses. Stations NOR and NRC are located within the Norcia basin, while T1212 is placed on outcropping bedrock. Cross sections AA' and BB', also referred to as P1 and P2, respectively, are shown in detail in Figure 2.

Profile P1 is NS oriented and 8 km long, while P2 has an azimuth of 77.34° and 6.7 km long. Note that the latter follows exactly the geological profile constructed by recent microzonation studies (Motti, 2017). Furthermore, the maximum sediment thickness for profile P1 and P2 are nearly 400 m and 360 m whereas the maximum basin widths are 4600 m and 3660 m respectively. It is also worth noticing the marked geometrical difference between the two profiles. The shape of profile P1 le is more symmetrical presenting its deepest portion at its center. On the other hand, profile P2 has a less narrow shape and it is considerably more asymmetric with its sediment cover thickening towards the east.

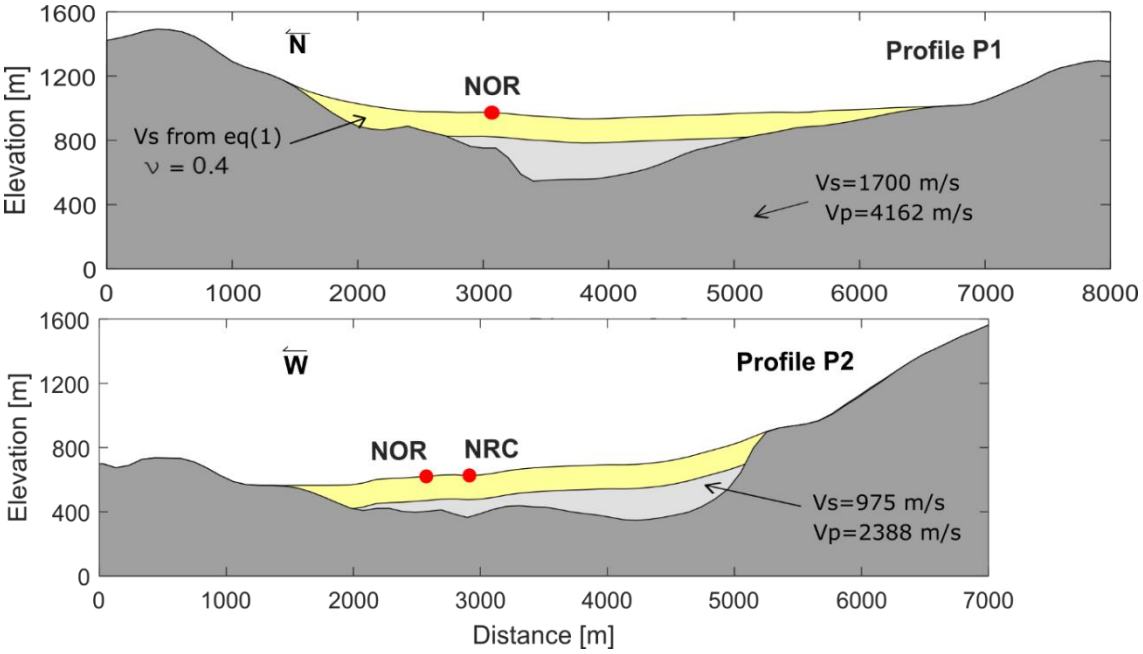

Figure 2. Schematic of Profiles P1 (top) and P2 (bottom). Red points indicate the locations of the NOR and NRC stations. V_S and V_P values of the bedrock and alluvial sediments are also displayed.

3. Aggravation factors for 2D site effects in basin geological configurations

As previously mentioned, at a given site, 2D Period Dependent Aggravation Factors (PDAF) were defined as the ratio between the 2D and 1D corresponding spectral accelerations (SA). As it is evident, the PDAFs also vary according to location *x* on the basin free surface and hence, they are expressed as follows:

$$PDAF_{(T,x)} = \frac{SA_{2D(T,x)}}{SA_{1D(T,x)}} \quad (3)$$

The quantification of PDAFs on ground motion intensity measures other than SA (e.g. Arias Intensity, etc.) can also be found in the literature (e.g. Gelagoti et al., 2010; Moczo et al., 2018, amongst others). Nonetheless, this study focuses on PDAF expressed in terms of spectral acceleration (SA), as shown by Eq. (2), because of its direct relation with the definition of seismic action in modern seismic building codes.

As explained by Bard and Bouchon (1980), the 2D response of sediment filled valleys is controlled by the back and forth propagation of basin edge induced surface waves and their subsequent interaction with the refracted wavefield. For *deep valleys*, the interaction among surface waves can degenerate into 2D resonance patterns, yet, evidence of 2D resonance effects is rather scarce (Faccioli and Vanini, 2003). For *shallow basins*, the constructive interference between the refracted body waves and the edge-induced surface waves is the main cause of ground motion amplification, particularly at the near edge regions. Thus, the term *edge effect* has been commonly used to refer to such type of phenomena (Kawase, 1996). Nonetheless, the ground shaking produced by basin induced surface waves can be dependent on several other path and source effects/factors (e.g. back-azimuth, forward directivity; Bradley, 2012)

The zone where the edge effect develops is expected to be closer to the edge in the case of high frequency motion, and the opposite for low frequency motion (Gelagoti et al., 2010b; Hallier et al., 2008; Paolucci and Morstabilini, 2006). Particularly, for trapezoidal basins, ground motion aggravation given by the edge effect was identified to occur partially or totally outside the edge wedge. This zone is either preceded or followed by a zone where deaggravation or no aggravation occurs as it has been evidenced from numerical studies of idealized shallow basins (Zhu et al. ,2018b; Riga et al., 2016, Narayan and Singh, 2006) and from 3D or 2D analysis of actual basins (Bradley, 2012b; Hasal et al., 2018; Madiai et al., 2017b; Sun and Chung, 2008).

4. Methodology

To evaluate the seismic response of the Norcia basin, 2D linear visco-elastic (LVE) wave propagation analyses were performed using the commercial program FLAC 2D (Itasca, 2007). The code implements an explicit Finite Difference (FD) scheme to fully solve the equations of motion in time domain. On the bottom and lateral boundaries of the models, proper absorbing and free-field boundary conditions can be specified by the user. The features of the finite difference grids implemented for each profile are reported in Table 1. One-dimensional ground response analyses were also carried out using the same code on the 1D soil column extracted below each receiver, which were positioned nearly every 100 m on top of the sediments.

Table 1. Characteristics of the grids used in FLAC for profiles P1 and P2

Profile	Extension [Km]	N. of elements	Max. element length [m]		Max. Frequency [Hz]
			For sediments	For bedrock	
P1	8.00	118446	5	35	5
P2	6.75	83739	5	35	5

A preliminary study was carried out by considering vertically propagating incident plane SV motions represented by both the Gabor and the Ricker wavelets (Figure 3). The former has an almost constant Fourier Amplitude Spectrum (FAS) up to 5 Hz, while the Ricker pulse was centered around the 1D fundamental frequency (f_{c1D}) which is estimated for the central portion of the two profiles around 0.8 Hz. These simulations were carried out to capture the main physical mechanisms involved in the 2D response of the selected profiles and to analyze the effect of frequency content of the input excitation on the PDAFs.

Additional analyses were performed to explore the dependence of the aggravation factors on the irregularities of the geometry of the sediment basement. For this purpose, simplified cross-sections with "regularized" interfaces were generated for both P1 and P2 profiles (see Figure 4). These are hereinafter referred with the acronyms S1P1 and S1P2, respectively. In the case of P1, the sediment thickness was approximated to an acceptable degree however the topography was not included. As for P2 , the simplification assumes a trapezoidal shape for the sediment cover with a slightly sloping sediment basement; topography in this case was also approximated with a gentle slope of 4°.

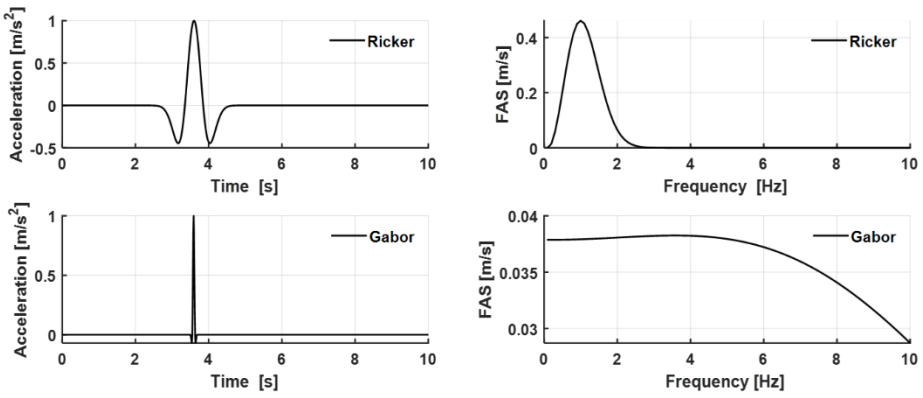

Figure 3. Gabor (top) and Ricker (bottom) wavelets used as input excitations (SV vertical plane wave) for the preliminary 2D simulations performed with FLAC2D.

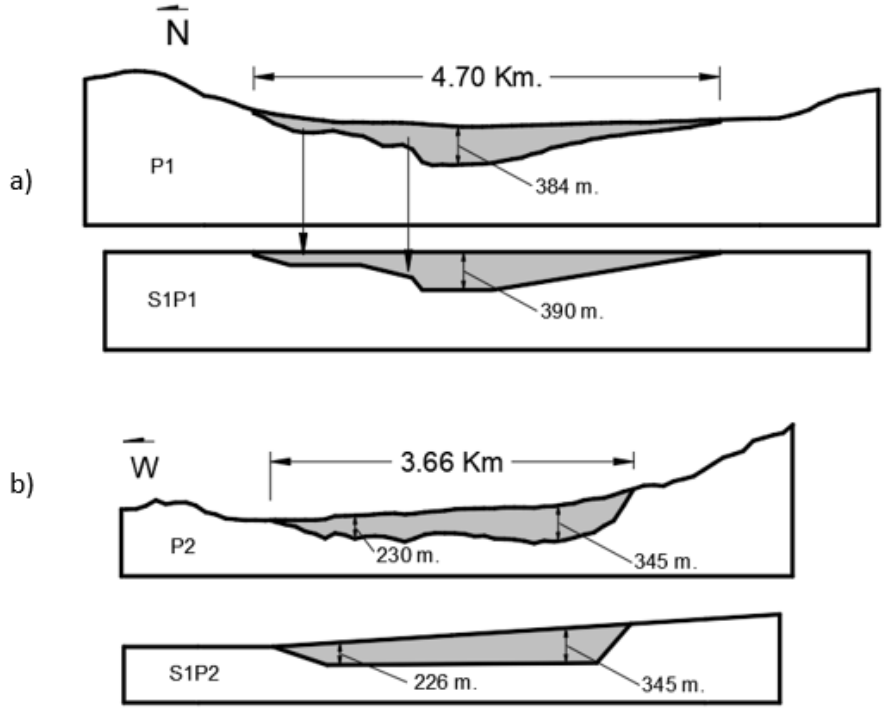

Figure 4. Geometry of the "simplified" profiles used to study the effect of the irregularity of the sediments-bedrock interface on the PDAFs. a) Profile P1 and the simplified profile S1P1. b) Profile P2 and the simplified profile S1P2.

The effect of damping ratio and the non-linear response of the sediments was further examined by considering as seismic excitation the horizontal ground motions recorded at the station T1212 (see Figure 1) during the OCT/30 2016 main shock of Mw6.5 .To account for geometric attenuation due to the different source-to-site distances at T1212 and NOR stations, the horizontal recordings were linearly scaled to a PGA of 3.25 m/s^2 corresponding to the median prediction of the Ground Motion Prediction Equations of Bindi et al. (2011), for hypothetical rock conditions at the NOR site. The corresponding acceleration time histories and acceleration FASs are shown in Figure 5. For profile P1 the NS component of the recording was used while for P2 the horizontal motion was rotated to the corresponding azimuth.

For the LVE analysis, material damping is modelled according to the Rayleigh's mass and stiff proportional damping approach. For the present case, the Rayleigh damping parameters were selected in such way that the target hysteretic damping is maintained valid between 0.2 and 5 Hz. The complete set of parametric numerical analyses performed in this work is summarized in Table 2.

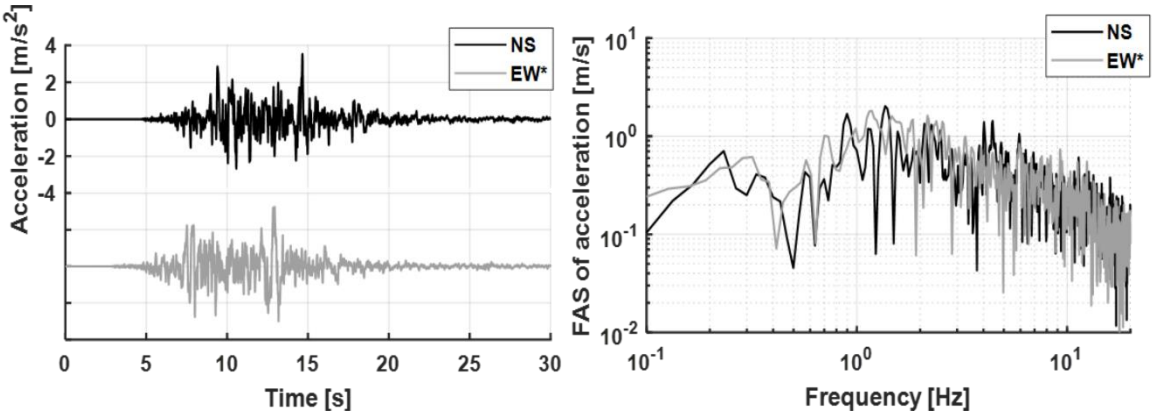

Figure 5. Left, scaled acceleration time traces from the recordings made at the station T1212 (see Figure 1) along the NS and EW directions. The latter corresponds to an azimuth of 77.34°. Right, acceleration Fourier amplitude spectra for both components.*

Table 2. Summary of numerical analyses performed in this study for the estimation of PDAFs for the Norcia basin.

Incident motion	**Material behavior**	**Profiles**
Gabor	Linear viscoelastic ξ = 1%	P1-S1P1-P2-S1P2
Ricker	Linear viscoelastic ξ = 1%	P1-S1P1-P2-S1P2
T1212	Linear viscoelastic ξ = 1%	P1-P2
T1212	Linear viscoelastic ξ = 2%	P1-P2
T1212	Linear viscoelastic ξ = 3.5%	P1-P2
T1212	Non-linear FLAC-HYST	P1-P2

To calibrate the non-linear analyses (see last row in Table 2), the shear modulus degradation (G/G_{max}) and damping (ξ) curves were generated according to the model proposed by Darendeli (2001). Undisturbed samples were recovered during a field exploration campaign executed to the north west of the basin, near the town of Norcia. Results of two resonant column tests were used to calibrate the final model, which is displayed in Figure 6 by black lines. As a more detailed geotechnical characterization of the sediments cover over depth was not available, these properties were assigned to all the sediments layers. In FLAC non-linear analyses, referred to as "hysteretic analysis" or HYST, were also performed, for which the shear modulus and damping curves are those depicted in Figure 6.

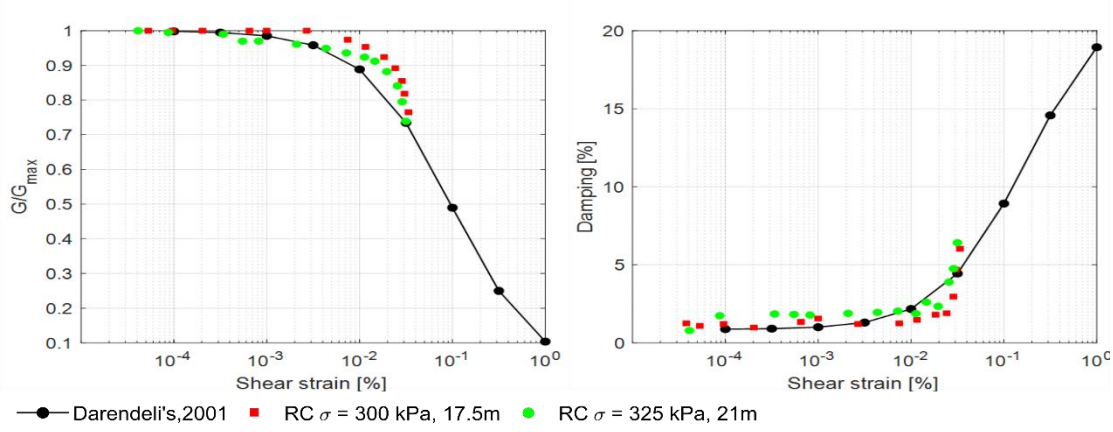

Figure 6. Calibration of shear modulus degradation (left) and damping ratio (right) curves adopted for hysteretic FLAC2D analyses. The scatter points correspond to the results of two resonant column (RC) tests, performed on samples retrieved at 17.5 and 21 m near the town of Norcia, under confining pressures (σ) of 300 and 325 kPa.

5. Overview of 2D linear viscoelastic response

From the initial wavelet-based analyses, the 2D and 1D responses of profile P1, in terms of acceleration synthetics, are shown in Figure 7 and Figure 8, Figure 8. Acceleration synthetics obtained from the 2D (horizontal-x and vertical-z components) and 1D LVE analyses on P1, excited with the Ricker pulse.for Gabor and Ricker wavelets respectively. The first two panels depict the horizontal and vertical components of the acceleration wave-field obtained at the basin surface of each profile. Similarly, the third panel shows the 1D response for each soil column that constitutes the basin beneath each receiver. It is worth to recall that wavelet peak frequency of the Ricker wavelet (0.8 Hz) was selected to be close to f_{c1D} .

As it can be noticed for the Gabor case (Figure 7) the 2D response of P1 is controlled by the propagation of different trains of edge-induced surface waves, which are absent in the 1D response. At least three different modes of Rayleigh waves can be noticed to emanate from the edges, where their interaction with the direct/refracted arrivals mainly occurs. At the central region of the profile several collisions/constructive interferences among surface waves resulted in an important prolongation of the ground motion.

For the Ricker wavelet incidence, the acceleration synthetics depicted in Figure 8 show that the edge-generated Rayleigh waves are in this case capable of traveling through the entire basin carrying more energy with lower attenuation. They collide at the basin center, which results in a ground motion enhancement, compared to the 1D case. Furthermore, the vertical motion component shows that several phase reversals take place at the basin center caused by the collisions among the aforementioned surface waves. Such response may resemble a 2D resonance pattern similar to those described by Bard and Bouchon (1980) and Roten and Fäh (2007), who showed that the resonant behavior of a sediment-filled valleys is dominated by the reverberation of these edge-induced surface waves, that in the case of low frequency excitations, and for deep valleys, can degenerate into 2D resonance patterns. On the other hand, for shallow valleys, 1D resonance together with the back and forth propagation of the edge-induced surface waves is instead expected to be the dominant resonance pattern. However, these two types of resonant responses, as described by Bard and Bouchon (1980), are featured by two extreme cases, and the constructive interference of the surface waves on the valley center is always present, but only becomes predominant if the basin is particularly deep. In such scenario, the fundamental frequency is almost the same for the entire basin, opposite to the present case. As it will be later shown, the present case could be a good example of an *intermediate* response of a relatively shallow basin for which the edge-induced surface waves play an important role through its entire extent. Similar results about the importance of these low frequency surface waves were also obtained by Gelagoti et al. (2010) and Harsem and Harding (1981) for shallow trapezoidal basins.

Given that the previous observations are also valid for profile P2 (not shown here for brevity), we limit ourselves to show in Figure 9 the amplification functions (i.e. the ratio between surface and outcropping-rock acceleration FAS) computed for each profile and for both 2D and 1D analyses.

It is clear from Figure 9 that the 2D fundamental frequency ($f_{c,2D}$) is around 0.75 Hz for both P1 and P2, reaching amplification values of $A_{2D}(f_{c,2D}) \approx 3$ and ≈ 3.5, respectively. When comparing the 2D and 1D fundamental modes, it is found that their nodal lines are almost coincident, suggesting that the basin behavior resembles that of a shallow basin. However, important disagreements are found in terms of amplification maxima, since the ratio A_{2D} ($f = f_{c,2D}$) / A_{1D} ($f = f_{c,1D}$) is nearly 1.3 and 1.5 for P1 and P2, respectively.

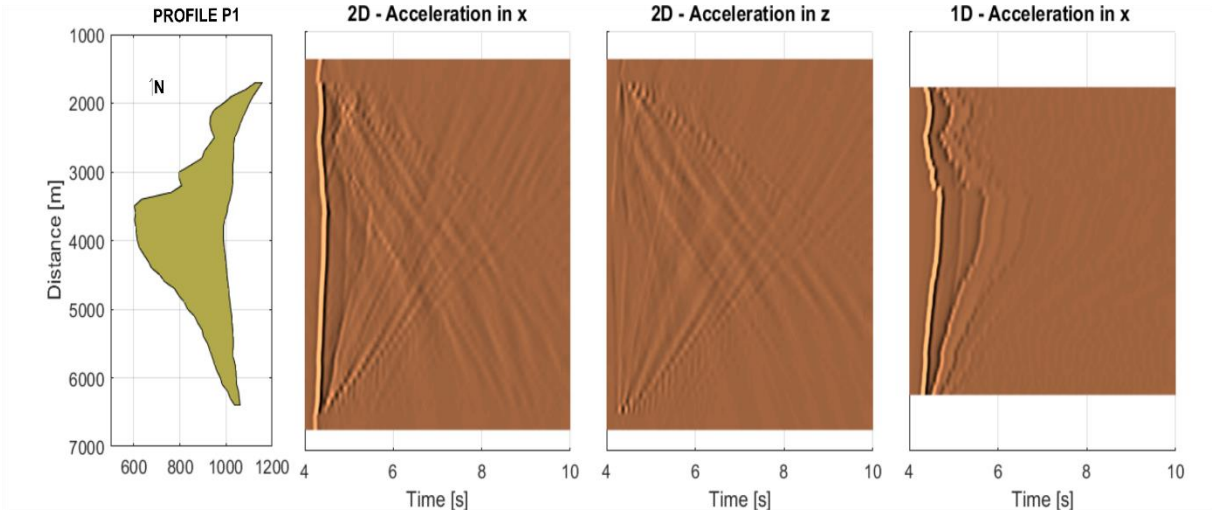

Figure 7. Acceleration synthetics obtained from the 2D (horizontal-x and vertical-z components) and 1D LVE analyses on P1, excited with the Gabor pulse.

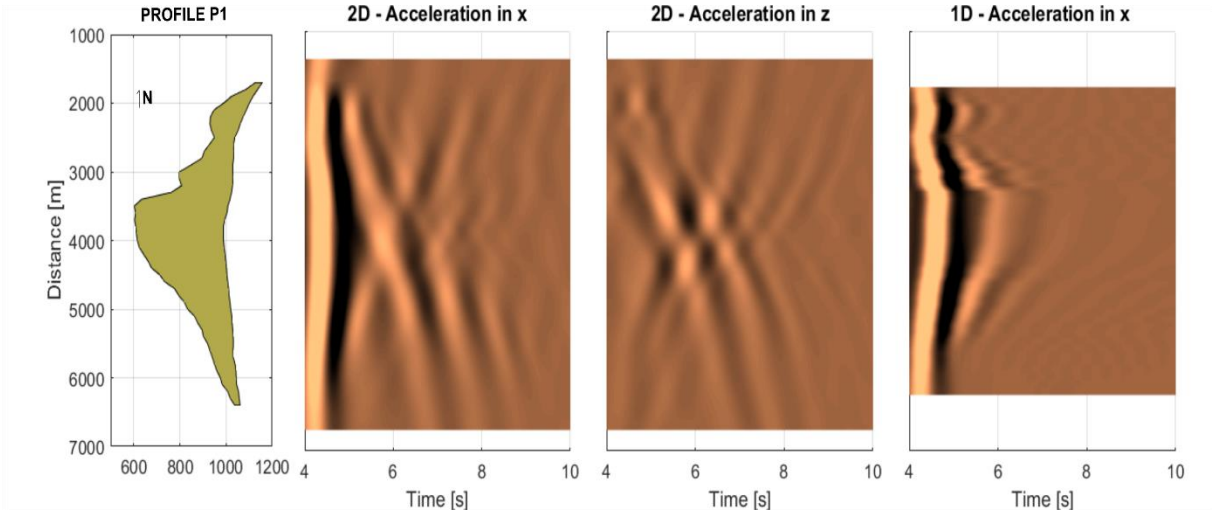

Figure 8. Acceleration synthetics obtained from the 2D (horizontal-x and vertical-z components) and 1D LVE analyses on P1, excited with the Ricker pulse.

The results of the 2D analyses also exhibits an additional important feature related to the extension of the amplification peaks. In Figure 9, the areas enclosed by dashed lines belong to the fundamental and first higher modes peaks for which $A_{2D} / A_{1D} > 1$. In the case of the fundamental mode, it can be noticed that its extension spans over a wide distance towards the edges, especially for profile P1. Similarly, and just in case of P1, the first 2D higher modes are also sufficiently wide to cover some portion of the basin center. If the extent of the fundamental mode and first higher modes of P1 spanned over the entire basin, it would completely coincide with the response of a deep basin such as the Rhone valley, as shown by Roten and Fäh (2007).

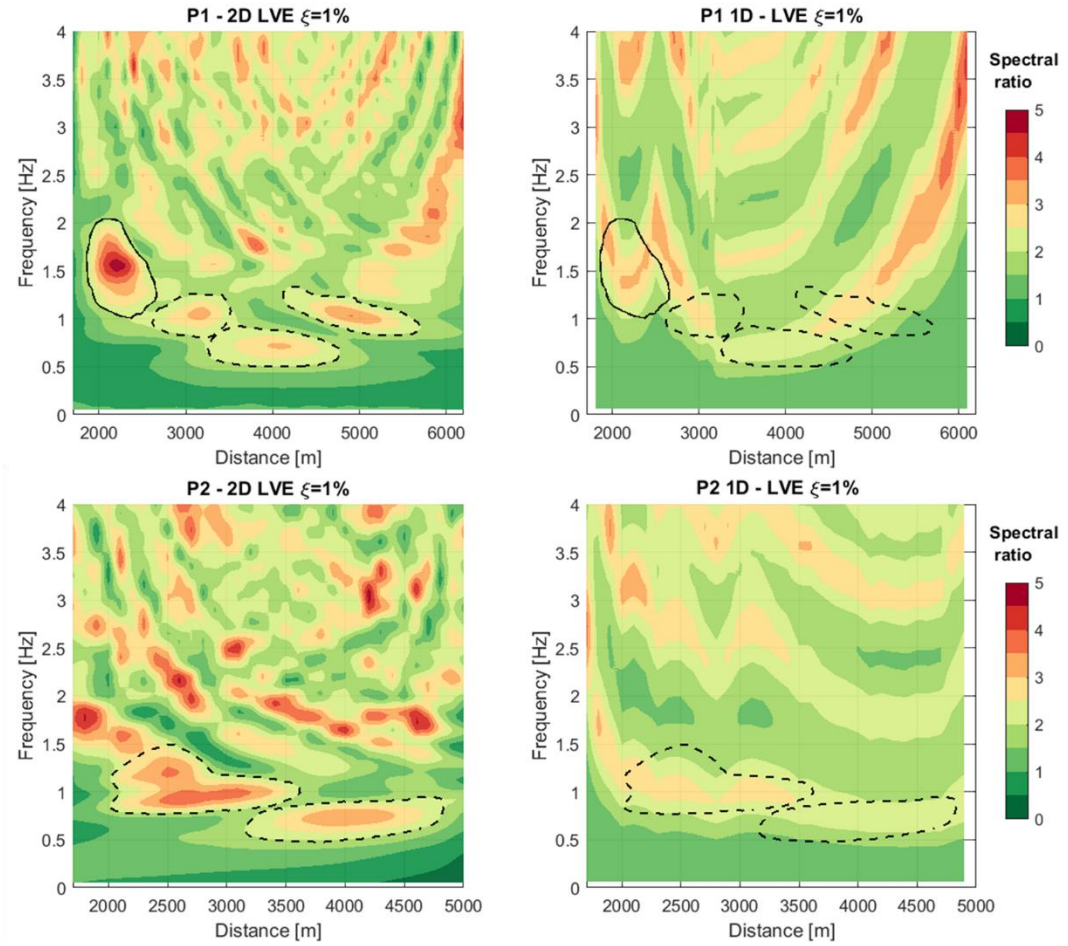

Figure 9. Spatial distributions of the 2D (left) and 1D (right) amplification functions computed for profile P1 (top) and P2 (bottom) under LVE behavior. Dashed and solid line contours enclose the prominent 2D amplification peaks.

Another relevant feature of the 2D amplification pattern of profile P1 is the strong amplification peak located at the northern edge sub-depression and enclosed by a solid line on the top left panel of Figure 9. It is found between 1.6 Hz and 1.7 Hz, corresponding to an amplification almost equal to A_{2D} (1.6 Hz) ≈ 5. In contrast, the 1D analysis shows an amplification around A_{1D} (1.6 Hz) ≈ 3.5. Such difference arises from the fact that in this region, wave-focusing mechanisms together with the propagation of edge-induced surface waves led to a more complex response.

For higher modes, the amplification pattern depicted by the 2D analyses is markedly different to that of the 1D analyses. In particular, compared to the 1D case, the distribution of nodal lines in the 2D case is characterized by the occurrence of several successive amplification peaks at higher frequencies and towards the southern and eastern edges for profiles P1 and P2, respectively. Such discontinuous or interfering amplification pattern is in accordance with the description of the resonance response of sediment-filled valleys present in the literature for idealized (Bard and Bouchon, 1985; Bielak et al., 1999) and real basins (Adams et al., 1999; Jongmans et al., 1998; Makra et al., 2002). Moreover, when comparing the 2D and 1D amplification patterns at higher frequencies (f > 1.2 Hz), P2 exhibits a stronger 2D amplification, while for P1 the 1D and 2D responses reach similar amplification values.

6. Aggravation factors

The 2D wave propagation phenomena analyzed in the previous Section, which may cause stronger amplification with respect the 1D case, are primarily due to the lateral variability of the bedrock depth across the basin. To study the role played by the basin geometry, this Section aims at comparing the PDAF found from the original profiles (P1 and P2) with those from the "simplified" ones with smoothed basin-bedrock interface (S1P1 and S1P2, see Figure 4 and Table 2). The discussion below will focus on the comparison P1-S1P1 profiles but similar conclusions can be inferred for P2-S1P2 profiles, because their response is governed by similar wave propagation phenomena.

In terms of amplification, the most significant differences are found for the northern edge (between 2 and 3 km), where the sub-depression is located. The fundamental mode on this region was found between 1.6 Hz and 1.7 Hz, with a peak amplification around 4 and 3.2 for P1 and S1P1, respectively. Furthermore, the 1D analyses indicate amplifications levels for this region are nearly equal to $A_{(f)}$ =2.8 for both profiles, fairly close to the values given by S1P1-2D. Therefore this can be interpreted as if most of the amplification at this zone is due to the shear wave velocity contrast, and that the additional amplification reported by P1-2D is then related to the focusing of incoming waves given the *convex* shape of the northern near edge zone.

Figure 10 shows the maps of PDAFs, computed according to Eq. (3), for P1 (left) and S1P1 (right), under the Gabor (top) and Ricker (bottom) wavelets. The aggravation was mostly controlled by the low frequency motion, being the maxima of the PDAF distribution of 5Hz Gabor wavelet almost unchanged on the 0.8 Hz Ricker wavelet analysis. Three different regions of important ground motion aggravation are identified, namely: between 2 and 2.5 km, 3 and 4.5 km and 5 and 6 km. With the exception of the latter, these regions corresponds to the amplification zones previously identified in Figure 9.

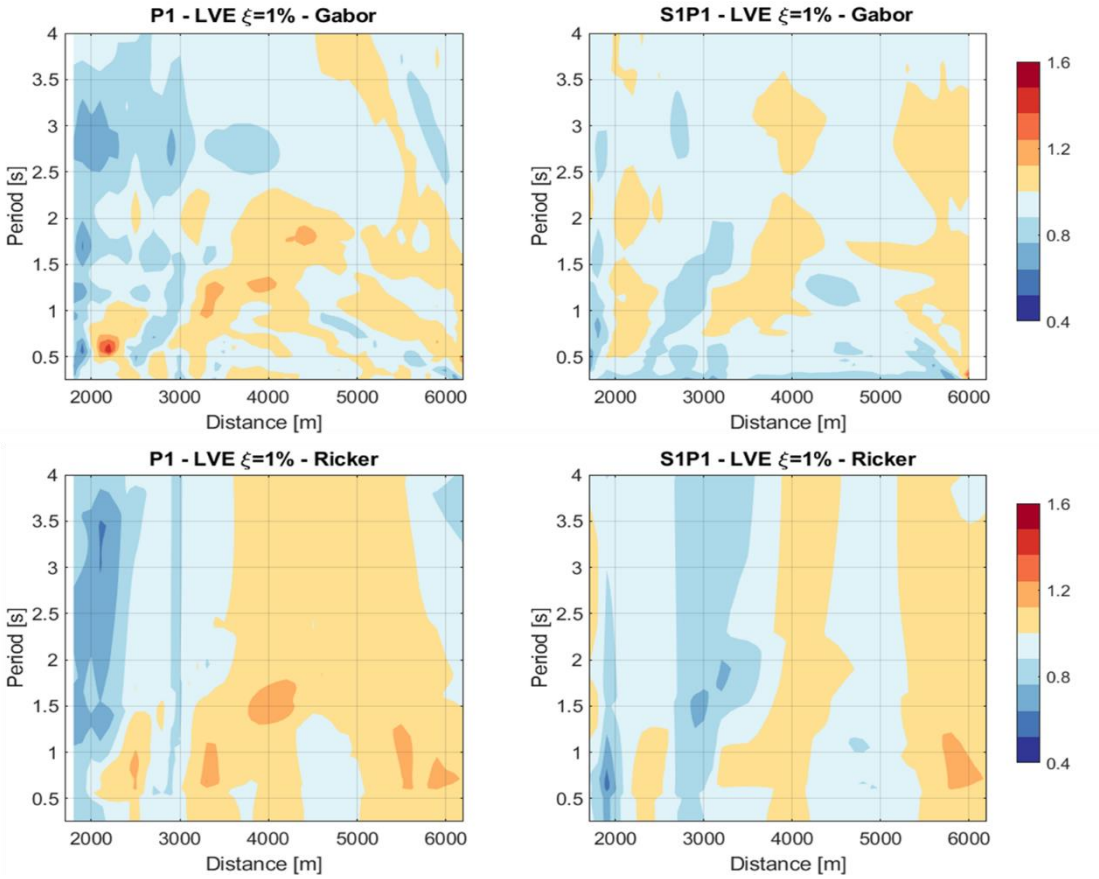

Figure 10. Spatial distributions of the PDAFs for P1 (left) and S1P1 (right) under Gabor (top) and Ricker (bottom) wavelet analysis.

The following comments can be made on the zones where major aggravation factors occurs:

- Between 2 and 2.5 km (northern edge), aggravation is controlled by the complex interaction between the waveforms propagating on a relatively broad frequency range, namely the focusing of refracted/reflected waves and their interference with edge-induced Rayleigh waves. The PDAF reaches a maximum of 1.5 in the case of the Gabor pulse incidence, for periods around 0.6 s, which coincides with both $T_{0,1D}$ and $T_{0,2D}$. Moreover, for S1P1, PDAF was about 1.2, thus, the highly irregular convex shape of P1 resulted into a PDAF 25% larger.
- Between 3.3 and 4.5 km, in the central portion of the basin, collisions/constructive interferences between surface waves lead to PDAF > 1.2 for periods between 0.9 s and 1.4 s, below $T_{0,2D}$ (which in this zone is equal to $T_{0,1D}$). The results indicate that most of the aggravation was due to the arrival of two trains of low frequency Rayleigh waves for both S1 and S1P1. Nonetheless, for the simplified profile the amplitude of the surface waves was smaller.
- Between 5 and 6 km (southern edge), the fundamental mode of the Rayleigh waves emanating from the edges coincided with the second body waves arrival. This region is influenced more clearly by the so-called *edge effect*, which seems to be more pronounced for low frequency excitations, leading to PDAF around 1.3. The picture portrayed for S1P1 is remarkably similar, indicating that the simplified profile also exhibits almost the same type of basin-edge related aggravation factor.

If we now compare in a broader sense the results of P1 and S1P1, it is noted that for S1P1 the magnitude of the aggravation factors was not as critical as for P1, even though for both profiles the seismic response was heavily dominated by the edge-induced surface waves. Therefore, the introduction of some simplifications in basin geometry, which is typically hard to constrain, plays a role in reducing the values of PDAFs, leading to an important source of uncertainty. In the literature a similar situation was found by Makra et al. (2005) who performed a parametric analyses on the 2D response of a cross-section of the Mygdonian basin in Greece, by approximating the basin shape with two different trapezoids. It was found that, for the two simplified profiles, the effect of the edge-induced surface waves was significantly reduced.

The PDAF patterns found for P2 and S1P2 are compared in Figure 11 and indicate a similar aggravation pattern as found for P1-S1P1 profiles, with three main zones of maximum aggravation factors: one near both eastern and western edge (from 2 to 2.8 km, and from 4 to 4.7 km) and a wider area at the center (between 3 and 4 km). The aggravation peaks located at the near-edge zones are preceded by a de-aggravated area and followed by a decrease in PDAF towards the basin center, which is agreement with the edge-effect features described by Kawase (1996) and Zhu et al. (2019).

When comparing the Ricker wavelet PDAFs to those obtained for the Gabor pulse, it can be noticed that the aggravation peaks located at the edges were increased from 1.2 to 1.4 and from 1.1 to 1.3, for the western and eastern peaks, respectively. This implies that, for profile P2, the edge-effect is more pronounced for broad-frequency band excitation. Similar to the sub-depression of the northern edge of profile P1, the rather shallow sediments are indeed more susceptible to experience aggravation due to the incidence of waves carrying energy over a rather broad frequency band.

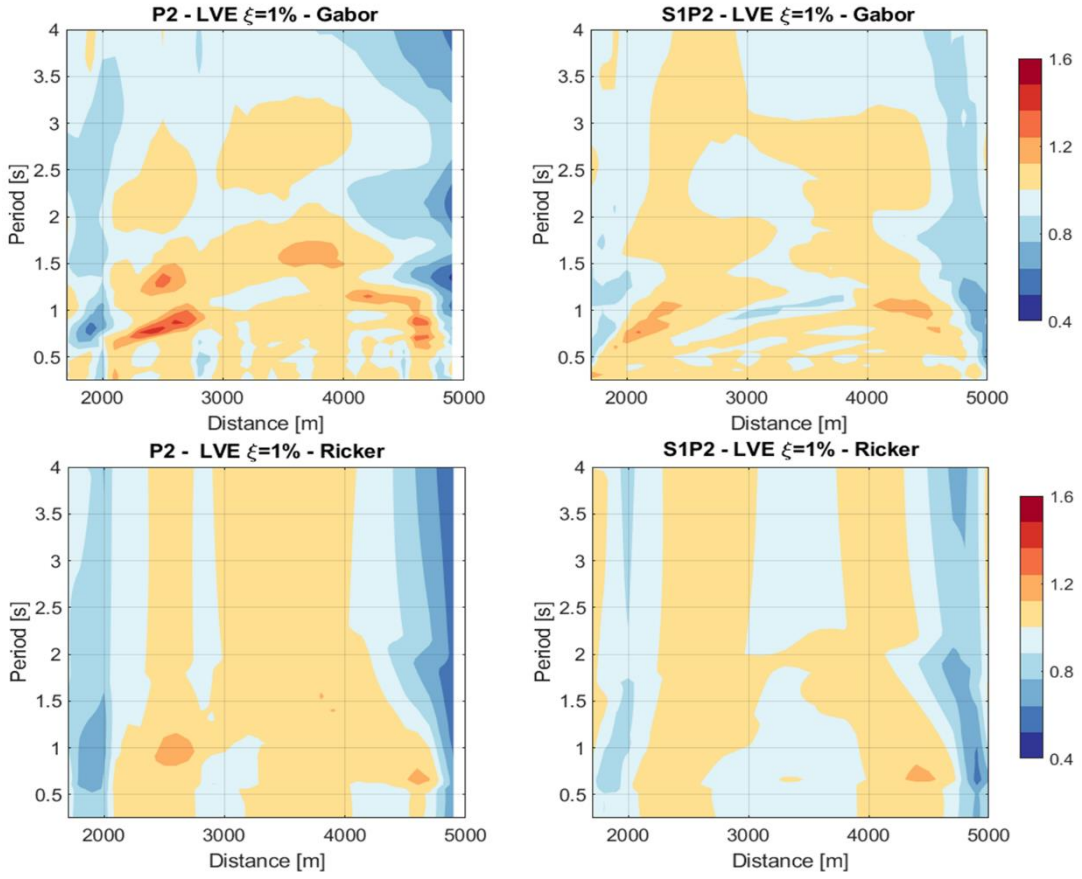

Figure 11. Same as in Figure 10 for P2 (left) and S1P2 (right).

From Figure 11 it is found that the overall PDAF pattern of S1P2 remarkably resembles that of P2, with the clear exception of the aggravation peak found in P2 between 3.5 and 4.0 km, absent in S1P2. However, there is a rather uniform underestimation of the PDAFs in the simplified profile, yet at a different extent for each wavelet analysis. Since the irregularity of the sediments-bedrock interface is less captured by longer wavelengths, the differences between P2 and S1P2 are more pronounced for the Gabor pulse, where the PADFs are approximately 15% lower for S1P2. This indicates that the aggravation factors are frequency-dependent, with P2 being more influenced by high frequencies, owing to, on one hand, to the dispersive nature of surface waves (see also Gelagoti et al., 2010; Zhu et al., 2018a), and to the other, to the complex interaction of refracted/reflected waveforms triggered by a high frequency motion with edge-induced surface waves.

As a whole, the most significant aggravation obtained for both profiles was around 0.5s < T < 1.5s. In the following, the sensitivity of the aggravation factors for the analyses reported in Table 2 will be presented in terms of the maximum PDAF for periods longer than 0.5s.

Considering that the 1D fundamental period in the central portion of the profiles ($T_{o,c}$) is estimated to be around 1.4 s and 1.25 for P1 and P2, respectively, the highest PDAFs are confined to the range of $0.4\ T_{o,c} < T < 1.2\ T_{o,c}$, which is consistent with the short period aggravation band proposed by Riga et al. (2016). Yet, most of the aggravation peaks tend to coincide with the 2D natural period at each particular location.

6.1 Effect of the type of incident motion

Besides the analyses with the Gabor and Ricker wavelets, the ground motion recorded during the 30-OCT main-shock was also used as vertically propagating plane SV excitation. The results in terms of maximum PDAF are depicted in Figure 12, for periods longer than 0.5 s. For P1, the 30-OCT event leads to higher PDAF values than the wavelets analyses, while for P2 the variation is more limited but still noticeable. The variability of the PDAF with respect to the input motion is indeed of foremost importance. However, the previously identified zones of PDAF maxima are present in all cases, indicating that similar constructive/destructive interference mechanisms occurred with the two types of input motions.

In general, the largest aggravation peaks spanning from PDAF = 1.2 to PDAF = 1.6, fall within the same range as found from the analyses performed on shallow basins by Zhu et al. (2018a) and Riga et al. (2016).

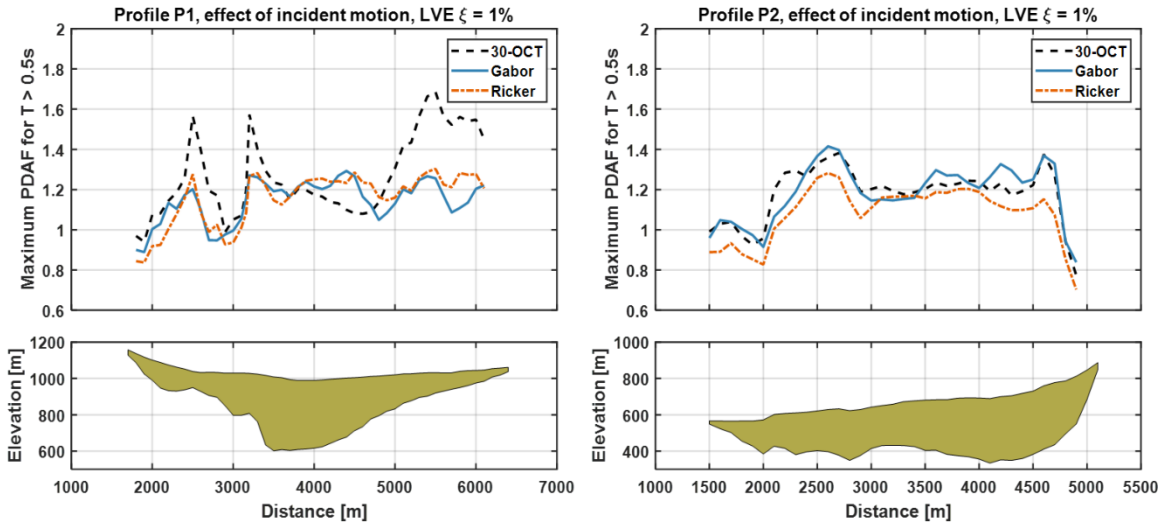

Figure 12 Effect of the type of incident motion on the maximum PDAFs for profiles P1 (left) and P2 (right).

6.2 Effect of the sediments-bedrock irregularity of the interface

As previously mentioned, the simplified cross sections (S1P1 and S1P2 in Figure 4) were generated to test the sensitivity of the PDAFs to the geometrical irregularity of the sediments cover. Since the previous section partially addressed this issue, the comparison will be now continued in relation to the 30-OCT motion. Figure 13 illustrates the correspondence between the maximum PDAF obtained for the *real* and simplified profiles (P1, left; P2: right). It can be noticed that the simplified cross sections led to smaller PDAFs, around 20 to 30 percent. Such reduction is even more noticeable in the case of profile P1. Initially, one may expect that a more regular shape of the sediments-bedrock interface (*s-br*) would mostly effect the short wavelength components, yet it also affected the low frequency motion, in particular the edge induced surface waves. This is likely due to the modification of other geometrical features more related to long wavelengths such as topography and slope of the sediments-bedrock interface at the basin edges.

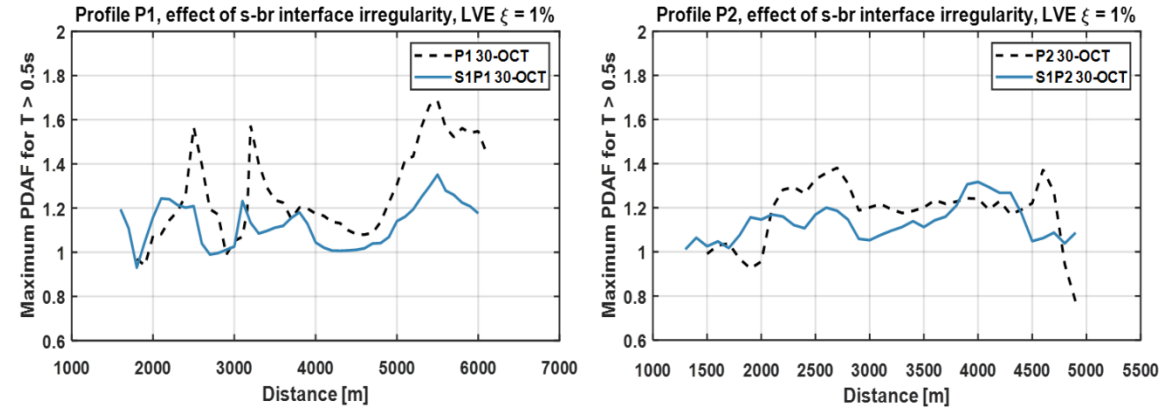

Figure 13. Comparison between the maximum PDAFs computed after the LVE performed on profiles P1-S1P1(left) and P2-S1P2 (right) with the 30-OCT as incidence motion.

6.3 Effect of damping ratio

This Section focuses on the effect of damping ratio on the ground motion aggravation factor in relation with the 30-OCT event. The results of the previous discussions were obtained for a target hysteretic damping ratio $\xi = 1\%$. The results presented hereinafter cover LVE analyses with $\xi = 2\%$ and $\xi = 3.5\%$.

Figure 14 illustrates the maximum PDAF obtained for the three different damping ratios. The overall aggravation is preserved and the main aggravation peaks are still captured. There is a rather small exception for P1, at 5.5 km, where the increasing damping ratio values led to a slight reduction of the PDAF peak. Such a limited dependence on the damping ratio may be due to the relatively low frequency nature of the aggravation found for both profiles, mainly influenced by the back and forth propagation of low frequency surface waves, less attenuated by material damping. It should be stressed that these analyses cannot be used to draw general conclusions, since the role of damping ratio is also controlled by the frequency content of the earthquake excitation, as described by Gelagoti et al. (2010).

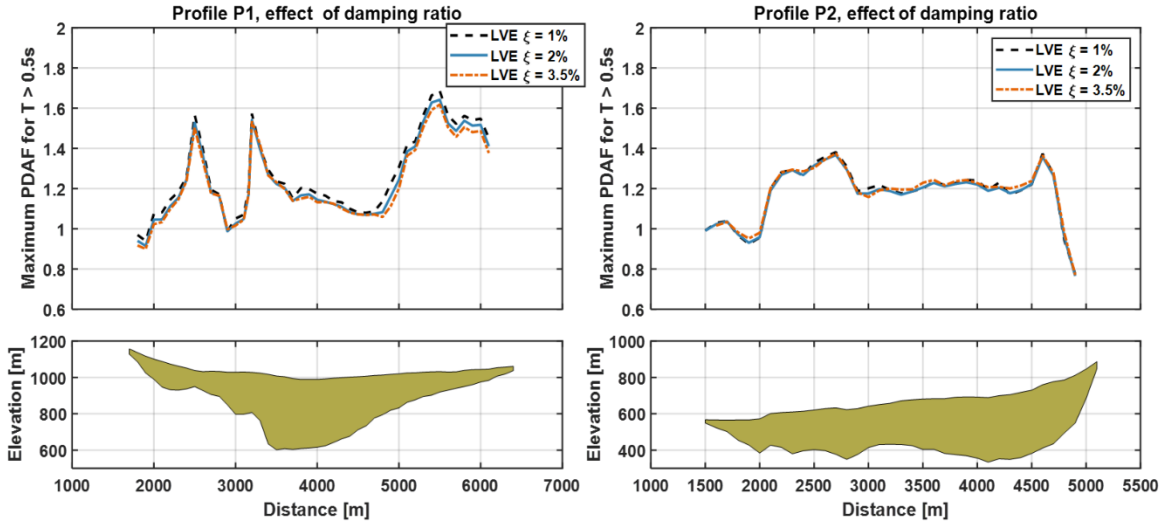

Figure 14. Effect of hysteretic damping on the maximum PDAFs computed after the LVE performed on profiles P1 (left) and P2 (right).

6.4 Effect of the non-linear ground response

The spatial variability of the maximum PDAFs obtained from the 2D and 1D non-linear (HYST) analyses are compared to those computed for the LVE $\xi = 1\%$ case in Figure 15.Figure 15. Comparison in terms of maximum PDAFs between the LVE and non-linear FLAC-HYST analyses. It is worth recalling that this work was not intended to fully address possible non-linear effects in the basin. Instead it aimed at identifying the general modifications that soil non-linearity may induce to 2D ground motion amplification.

The obtained results indicate that non-linearity not only affects the magnitude of the aggravation factors, but also shifted or enlarged the aggravation peaks. The different wave propagation mechanisms triggered by the 2D analyses, not captured by the 1D assessment, led to different level of strains and thus a significant disparity in terms of shear modulus reduction on the entire sediment

cover. In particular, the relatively high strains occurring at the interface between the bedrock and the sediments tend to favor the wave entrapment as well as to modify the directions along which the incoming seismic waves are refracted into the basin (Gelagoti et al., 2012). Such phenomena have the effect of altering the types of interferences/interactions between the different waveforms taking place near the basin surface, leading to larger or lower aggravation in some zones of the basin with respect to the linear case.

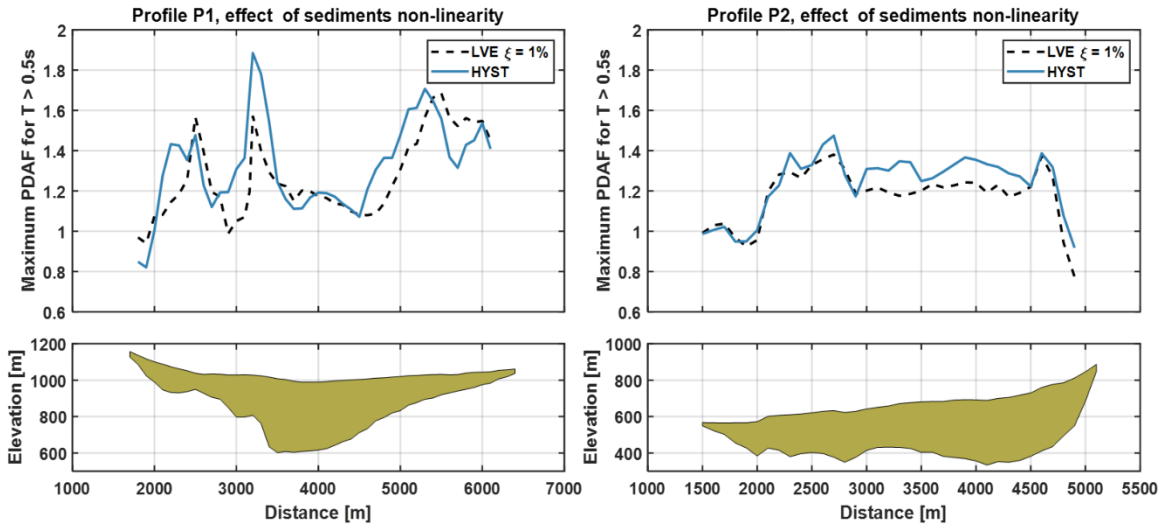

Figure 15. Comparison in terms of maximum PDAFs between the LVE and non-linear FLAC-HYST analyses.

7. Conclusive remarks

To estimate the PDAFs for the Norcia basin, time-domain linear visco-elastic and non-linear analyses were carried out on two different cross-sections of the basin with the finite difference commercial program FLAC2D. The excitation adopted for the analyses included a vertically propagating SV plane wave represented by Gabor/Ricker wavelets and an earthquake recording available at a near reference station during the M6.5 October 30, 2016 main-shock.

Although the Norcia basin is filled with relatively stiff sediments, the preliminary 2D wavelet analyses showed an increases of ground motion amplification and a shift of natural vibration modes towards lower frequencies with respect to the 1D case, owing to the generation of Rayleigh waves at the basin edges. These effects were particularly pronounced in the edge zones, where high PDAFs were obtained. In particular, for the fundamental and first higher modes, the amplification was found to be 30% to 50% higher in the 2D case.

The analyses performed under the earthquake recording indicated that the most significant aggravation (Figures 7.1 and 7.2) was found in the period range 0.5 s < T < 1.5 s, which is below the 1D fundamental period at the basin center ($T_{0,1D,c}$), estimated to be about 1.3 s. This finding is consistent with the findings of Chavez-Garcıa and Faccioli (2000), and Riga et al. (2016) about considering the basin effects for periods shorter than $T_{0,1D,c}$.

The set of sensitivity analyses performed by varying different assumptions including the input motion; the value of damping ratio; the geometry of the alluvial-bedrock interface; accounting for non-linear

soil response, allowed to draw the following conclusions on the mechanisms for site response aggravation in the Norcia basin:

- The response of the basin corresponds to that of a shallow basin, controlled by 1D resonance plus the propagation of edge-generated surface waves (Bard and Bouchon, 1985).
- The aggravation of profile P1 was found to be controlled by low frequency surface waves ($f < 1.0$ Hz), whereas for profile P2 the contribution of higher frequency components of ground motion was found to play a relevant role.
- The maximum PDAFs found at the near-edge regions were on the order of 1.4 and 1.6 for profiles P1 and P2, respectively, slightly larger than the mean long period values obtained by Riga et al. (2016) equal to around 1.3.
- Maximum PDAFs are within the same range as obtained in other case studies, such as the Mugello (Italy) and Mydgodonian (Greece) basins, for which values of 1.5-1.9 (Madiai et al., 2017; Zhu et al., 2018b) and of 2 were obtained (Raptakis et al., 2004).
- It was shown (Section 6.2) that simplifications of the geometry of the sediment-bedrock interface (roughness and/or bumpiness) may produce relevant changes in the distribution of maxima PDAF. In particular, smoother basin shapes led to a reduction of PDAF on the order of 30% for both profiles. A similar non-negligible variability was found for the SH case in a study performed by Makra et al. (2005) on the Mydgodonian basin.
- When accounting for non-linear response of the sediments, important changes on the PDAF spatial distribution were found (Figure 15), owing to the modification of the interaction between body and surface waves resulting from the concentration of shear strains along the contact zone between sediments and underlying bedrock (where a large impedance contrast occurs). This led to larger aggravation factors for some zones, and for others, de-aggravation, with a pattern similar to those found when the effects of input motion and alluvial-bedrock shape were considered alone.
- A rather limited impact of soil damping ratio (hysteretic in the seismic band of interest) was found. Yet, it was found that the frequency content of input motion as well as capturing the non-linear soil response play a non-negligible role on the calculated values of PDAFs.

As a final remark, it should be emphasized that the above considerations are based on a number of important limitations of the study including a) the assumption of only considering vertically propagating SV plane waves, b) a limited number of input motions and c) a single seismo-stratigraphic model for the sediment over and the bedrock. Further studies on 2D aggravation factors for the Norcia basin may therefore take into account the uncertainties associated with aforementioned assumptions.

Acknowledgements

This work was funded by the Italian Department of Civil Protection in the framework of the ReLUIS Research Project RS2. Authors would like to acknowledge the fruitful discussions made with Prof. Massimiliano Porreca and Dr. Maurizio Vassallo (University of Perugia), Dr. Francesca Pacor and Dr. Lucia Luzi (INGV, Milano) during the definition of the model of Norcia Basin and with Prof. Roberto Paolucci (Politecnico di Milano) in the discussion of results.

References.

Adams, B., Davis, R., Berril, J., Taber, J., 1999. Two-dimensional site effects in Wellington and the Hutt valley - Similarities to Hobe (Civil Engineering Research Report No. 99–03). Department of Civil Engineering, University of Canterbury, Christchurch, NZ.

Bard, P.Y., Bouchon, M., 1985. The two-dimensional resonance of sediment-filled valleys. Bulletin of the Seismological Society of America 75, 519–541.

Bard, P.-Y., Bouchon, M., 1980. The seismic response of sediment-filled valleys. Part 2. The case of incident P and SV waves. Bulletin of the Seismological Society of America 70, 1921–1941.

Bielak, J., Xu, J., Ghattas, O., 1999. Earthquake Ground Motion and Structural Response in Alluvial Valleys. Journal of Geotechnical and Geoenvironmental Engineering 125, 413–423. https://doi.org/10.1061/(ASCE)1090-0241(1999)125:5(413)

Bindi, D., Pacor, F., Luzi, L., Puglia, R., Massa, M., Ameri, G., Paolucci, R., 2011. Ground motion prediction equations derived from the Italian strong motion database. Bull Earthquake Eng 9, 1899–1920. https://doi.org/10.1007/s10518-011-9313-z

Bradley, B.A., 2012a. Strong ground motion characteristics observed in the 4 September 2010 Darfield, New Zealand earthquake. Soil Dynamics and Earthquake Engineering 42, 32–46. https://doi.org/10.1016/j.soildyn.2012.06.004

Bradley, B.A., 2012b. Strong ground motion characteristics observed in the 4 September 2010 Darfield, New Zealand earthquake. Soil Dynamics and Earthquake Engineering 42, 32–46. https://doi.org/10.1016/j.soildyn.2012.06.004

Chavez-Garcıa, F.J., Faccioli, E., 2000. Complex site effects and building codes: Making the leap. Journal of Seismology 4, 23–40. https://doi.org/10.1023/A:1009830201929

Chiaraluce, L., Di Stefano, R., Tinti, E., Scognamiglio, L., Michele, M., Casarotti, E., Cattaneo, M., De Gori, P., Chiarabba, C., Monachesi, G., Lombardi, A., Valoroso, L., Latorre, D., Marzorati, S., 2017. The 2016 Central Italy Seismic Sequence: A First Look at the Mainshocks, Aftershocks, and Source Models. Seismological Research Letters 88, 757–771. https://doi.org/10.1785/0220160221

Darendeli, M.B., 2001. Development of a new family of normalized modulus reduction and material damping curves. Ph.D. thesis, Univ.of Texas at Austin, Austin, TX.

Faccioli, E., Vanini, M., 2003. Complex seismic site effects in sediment-filled valleys and implications on design spectra. Prog. Struct. Engng Mater. 5, 223–238. https://doi.org/10.1002/pse.156

Galadini, F., Messina, P., Giaccio, B., Sposato, A., 2003. Early uplift history of the Abruzzi Apennines (central Italy): available geomorphological constraints. Quaternary International 101–102, 125–135. https://doi.org/10.1016/S1040-6182(02)00095-2

Galli, P., Galadini, F., Calzoni, F., 2005. Surface faulting in Norcia (central Italy): a "paleoseismological perspective." Tectonophysics 403, 117–130. https://doi.org/10.1016/j.tecto.2005.04.003

Gelagoti, F., Kourkoulis, R., Anastasopoulos, I., Gazetas, G., 2012. Nonlinear Dimensional Analysis of Trapezoidal Valleys Subjected to Vertically Propagating SV Waves. Bulletin of the Seismological Society of America 102, 999–1017. https://doi.org/10.1785/0120110182

Gelagoti, F., Kourkoulis, R., Anastasopoulos, I., Tazoh, T., Gazetas, G., 2010. Seismic Wave Propagation in a Very Soft Alluvial Valley: Sensitivity to Ground-Motion Details and Soil Nonlinearity, and Generation of a Parasitic Vertical Component. Bulletin of the Seismological Society of America 100, 3035–3054. https://doi.org/10.1785/0120100002

Graves, R.W., Pitarka, A., Somerville, P.G., 1998. Ground-Motion Amplification in the Santa Monica Area: Effects of Shallow Basin-Edge Structure. Bulletin of the Seismological Society of America 88, 1224-1242,.

Hallier, S., Chaljub, E., Bouchon, M., Sekiguchi, H., 2008. Revisiting the Basin-edge Effect at Kobe During the 1995 Hyogo-Ken Nanbu Earthquake. Pure and Applied Geophysics 165, 1751–1760. https://doi.org/10.1007/s00024-008-0404-y

Harsem, S., Harding, S., 1981. Surface motion over a sedimentary valley for incident plane P and SV waves. Bulletin of the Seismological Society of America 71, 655–67.

Hasal, M.E., Iyisan, R., Yamanaka, H., 2018. Basin Edge Effect on Seismic Ground Response: A Parametric Study for Duzce Basin Case, Turkey. Arabian Journal for Science and Engineering 43, 2069–2081. https://doi.org/10.1007/s13369-017-2971-7

Itasca, 2007. FLAC, Fast Lagrangian Analysis of Continua Version 7.0. Itasca Consulting Group, Minneapolis,.

Jongmans, D., Pitilakis, K., Demanet, D., Raptakis, D., Riepl, J., Horrent, C., Lontzetidis, K., 1998. EURO-SEISTEST: Determination of the Geological Structure of the Volvi Basin and Validation of the Basin Response. Bulletin of the Seismological Society of America 88, 473–487.

Kawase, H., 1996. The Cause of the Damage Belt in Kobe: "The Basin-Edge Effect," Constructive Interference of the Direct S-Wave with the Basin-Induced Diffracted/Rayleigh Waves. Seismological Research Letters 67, 25–34. https://doi.org/10.1785/gssrl.67.5.25

Luzi, L., Pacor, F., Puglia, R., Lanzano, G., Felicetta, C., D'Amico, M., Michelini, A., Faenza, L., Lauciani, V., Iervolino, I., Baltzopoulos, G., Chioccarelli, E., 2017. The Central Italy Seismic Sequence between August and December 2016: Analysis of Strong- Motion Observations. Seismological Research Letters 88, 1219–1231. https://doi.org/10.1785/0220170037

Madiai, C., Facciorusso, J., Gargini, E., 2017. Numerical Modeling of Seismic Site Effects in a Shallow Alluvial Basin of the Northern Apennines (Italy). Bulletin of the Seismological Society of America 107, 2094–2105. https://doi.org/10.1785/0120160293

Makra, K., Chávez-García, F.J., Raptakis, D., Pitilakis, K., 2005. Parametric analysis of the seismic response of a 2D sedimentary valley: implications for code implementations of complex site effects. Soil Dynamics and Earthquake Engineering 25, 303–315. https://doi.org/10.1016/j.soildyn.2005.02.003

Makra, K., Raptakis, D., Pitilakis, K., 2002. Site Effects and Design Provisions: The Case of Euroseistest. Earthquake Microzoning. Pageoph Topical Volumes. Birkhäuser, Basel. 2349–2367. https://doi.org/10.1007/978-3-0348-8177-7_5

Moczo, P., Kristek, J., Bard, P.-Y., Stripajová, S., Hollender, F., Chovanová, Z., Kristeková, M., Sicilia, D., 2018. Key structural parameters affecting earthquake ground motion in 2D and 3D sedimentary structures. Bull Earthquake Eng 16, 2421–2450. https://doi.org/10.1007/s10518-018-0345-5

Motti, 2017. Personal communications for the document: "Progetto cartografie geologiche e geotematiche delle aree terremotate finalizzate all'indifiduazione della pericolosità sismica locale-Sezioni 337010 'Serravalle' 337020 'Norcia' 325130 'Todiano' 325140 'Ancarano', Scala:1:10000."

Narayan, J.P., Singh, S.P., 2006. Effects of soil layering on the characteristics of basin-edge induced surface waves and differential ground motion. Journal of Earthquake Engineering 10, 595–614. https://doi.org/10.1080/13632460609350611

Özcebe, A.G., Smerzini, C., Paolucci, R., Pourshayegan, H., Rodriguez-Plata, R., Lai, C.G., Zuccolo, E., Bozzoni, F., Villani, M., 2019. On the comparison of 3D, 2D, and 1D

numerical approaches to predict seismic site amplification: The case of Norcia basin during the M6.5 2016 October 30 earthquake. Proceedings of the 7th International Conference on Earthquake Geotechnical Engineering (ICEGE 2019) 4251–4258.
Paolucci, R., Morstabilini, L., 2006. Non-dimensional site amplification functions for basin Edge effects on seismic ground motion. Preceedings of the third International Symposium on the Effects of Surface Geology on Seismic Motion 9.
Poceski, A., 1969. The ground effects of the Skopje July 26, 1963 earthquake. Bulletin of the Seismological Society of America 59, 1–22.
Raptakis, D., Makra, K., Anastasiadis, A., Pitilakis, K., 2004. Complex site effects in Thessaloniki (Greece): II. 2D SH modelling and engineering insights. Bulletin of Earthquake Engineering 2, 301–327.
Riga, E., Makra, K., Pitilakis, K., 2016. Aggravation factors for seismic response of sedimentary basins: A code-oriented parametric study. Soil Dynamics and Earthquake Engineering 91, 116–132. https://doi.org/10.1016/j.soildyn.2016.09.048
Roten, D., Fäh, D., 2007. A combined inversion of Rayleigh wave dispersion and 2-D resonance frequencies. Geophysical Journal International 168, 1261–1275. https://doi.org/10.1111/j.1365-246X.2006.03260.x
Sun, C.-G., Chung, C.-K., 2008. Assessment of site effects of a shallow and wide basin using geotechnical information-based spatial characterization. Soil Dynamics and Earthquake Engineering 28, 1028–1044. https://doi.org/10.1016/j.soildyn.2007.11.005
Yegian, M.K., 1994. Ground- Motion and Soil- Response Analyses for Leninakan, 1988 Armenia Earthquake. Journal of Geotechnical Engineering 120, 330–348.
Zhu, C., Riga, E., Pitilakis, K., Zhang, J., Thambiratnam, D., 2018a. Seismic Aggravation in Shallow Basins in Addition to One-dimensional Site Amplification. Journal of Earthquake Engineering 1–23. https://doi.org/10.1080/13632469.2018.1472679
Zhu, C., Thambiratnam, D., Gallage, C., 2019. Inherent Characteristics of 2D Alluvial Formations Subjected to In-Plane Motion. Journal of Earthquake Engineering 23, 1512–1530. https://doi.org/10.1080/13632469.2017.1387199
Zhu, C., Thambiratnam, D., Gallage, C., 2018b. Statistical analysis of the additional amplification in deep basins relative to the 1D approach. Soil Dynamics and Earthquake Engineering 104, 296–306. https://doi.org/10.1016/j.soildyn.2017.09.003

Figure1

Click here to download Figure Figure1.jpg

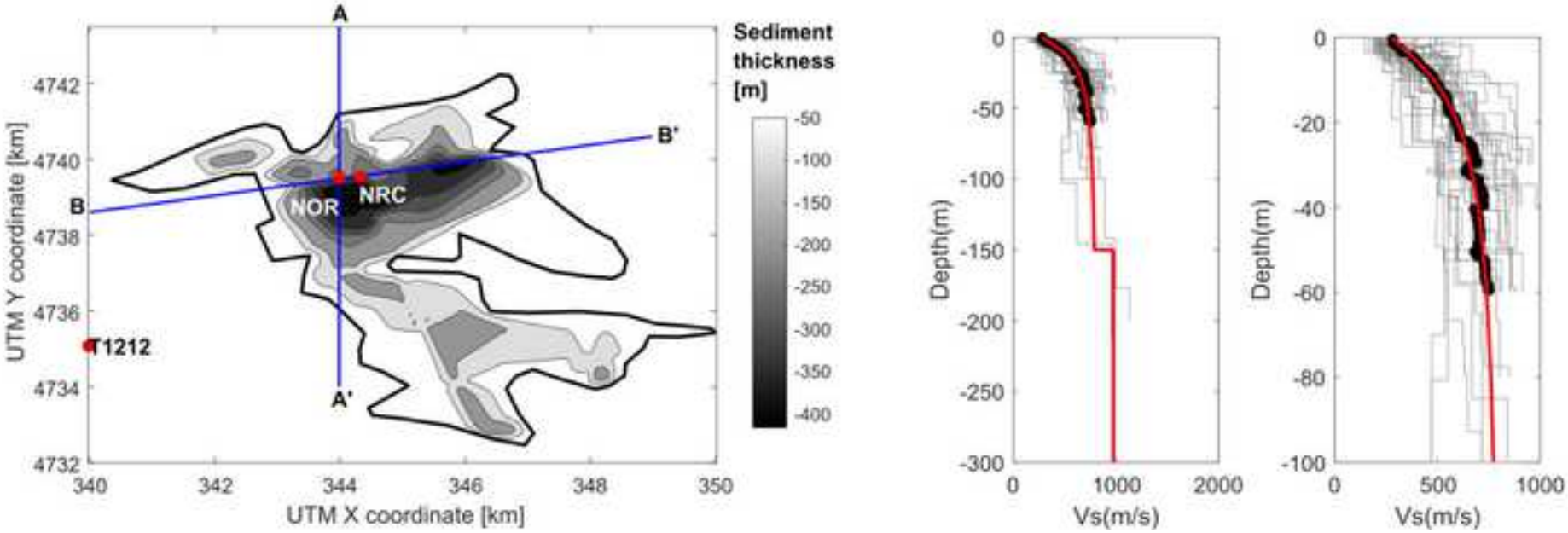

Figure2

Click here to download Figure Figure2.jpg

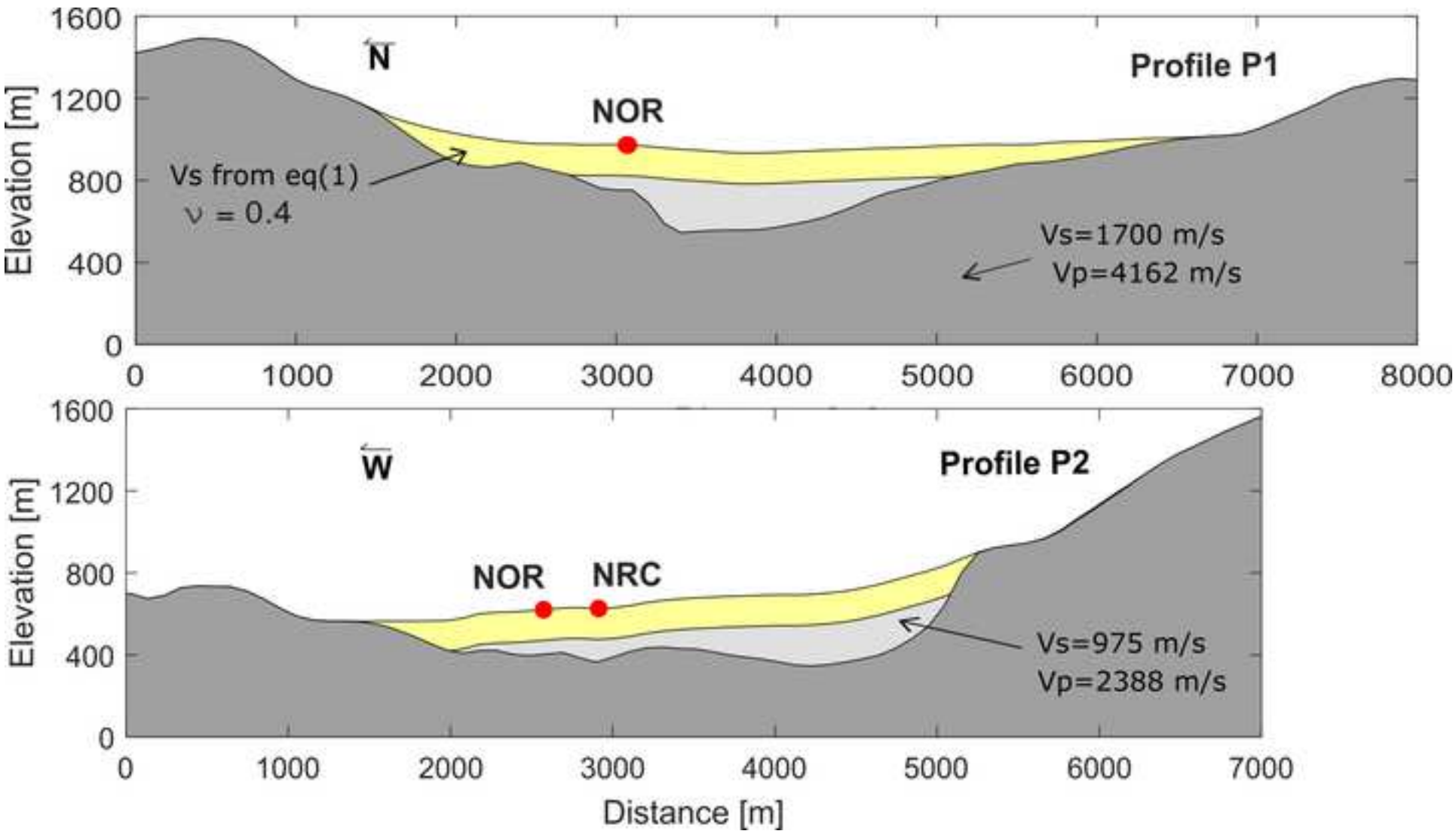

Figure3

Click here to download Figure Figure3.jpg

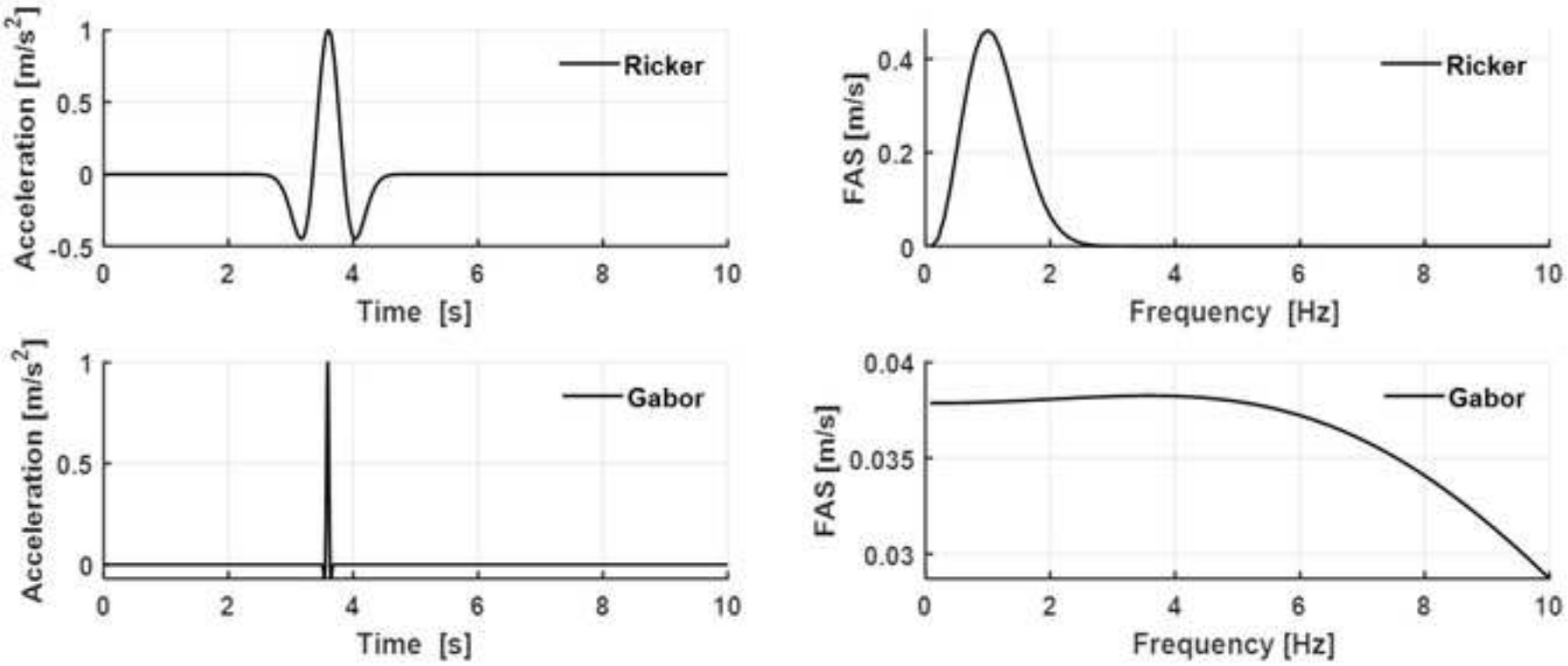

Figure4

Click here to download Figure Figure4.jpg

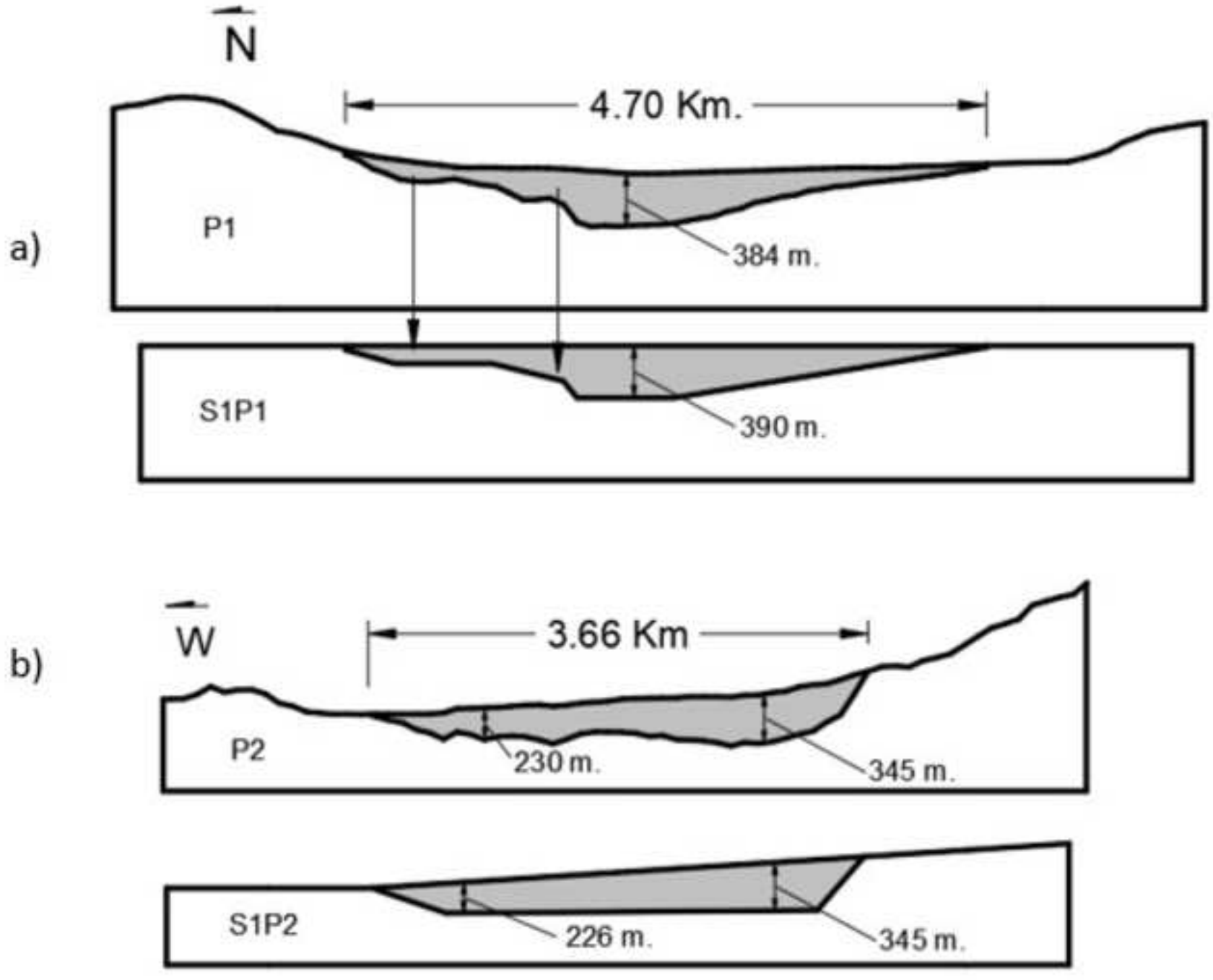

Figure5

Click here to download Figure Figure5.jpg

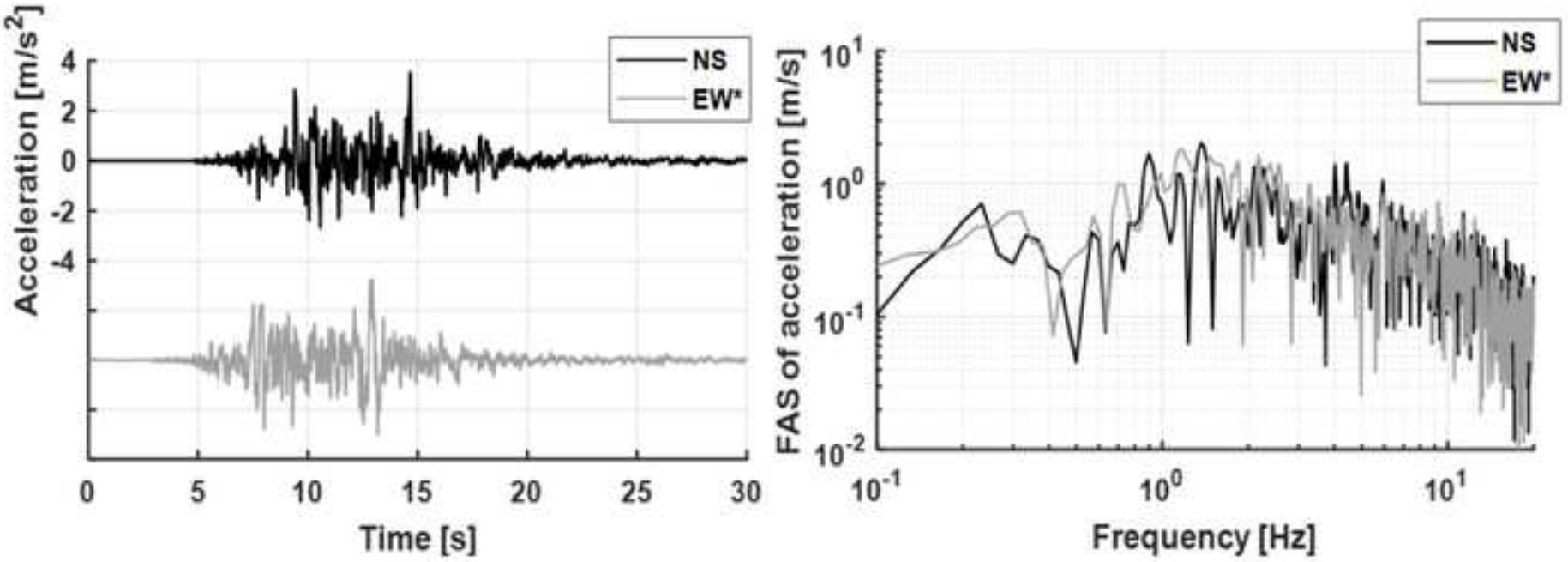

Figure6

Click here to download Figure Figure6.jpg

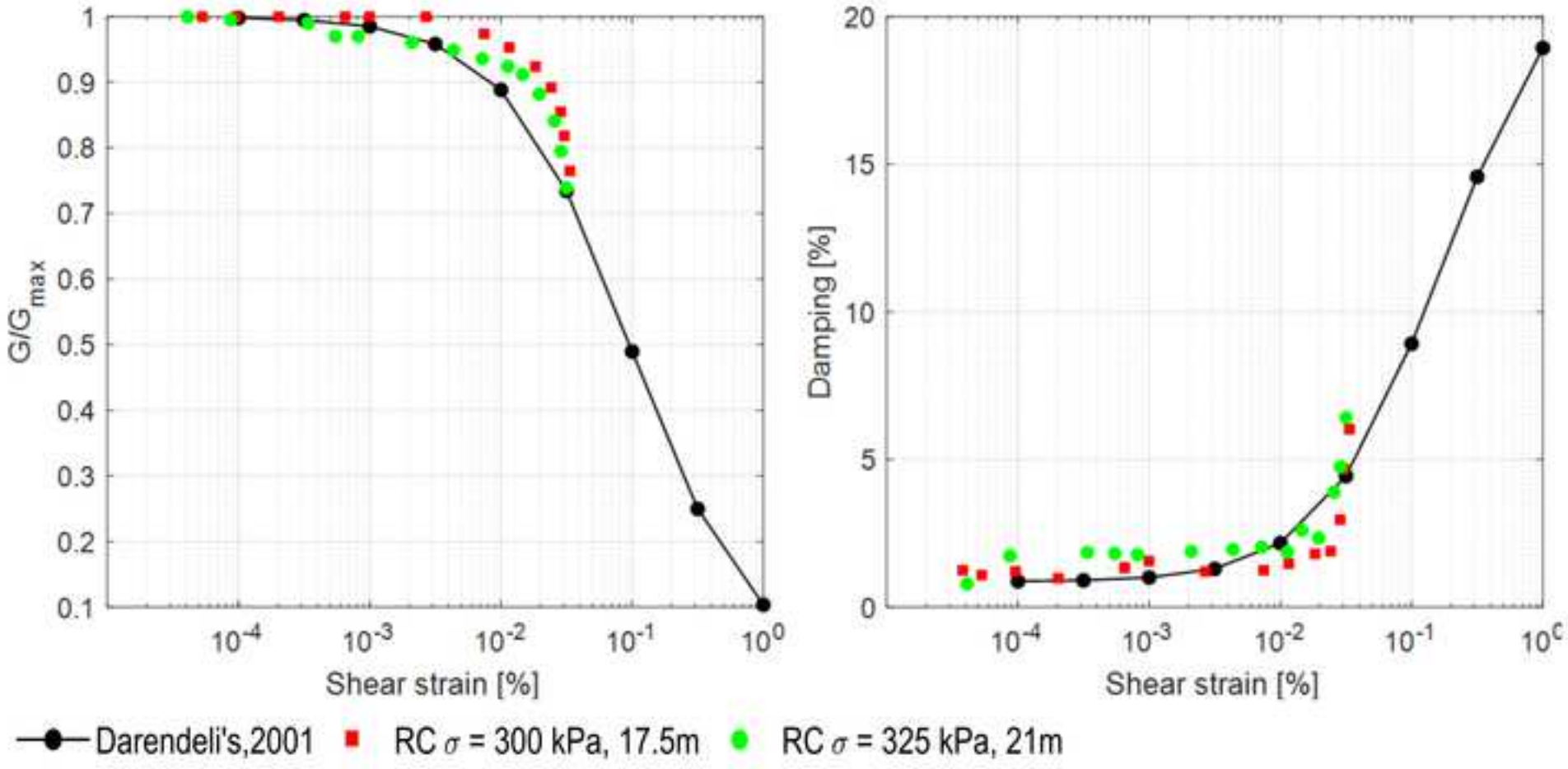

Figure7

Click here to download Figure Figure7.jpg

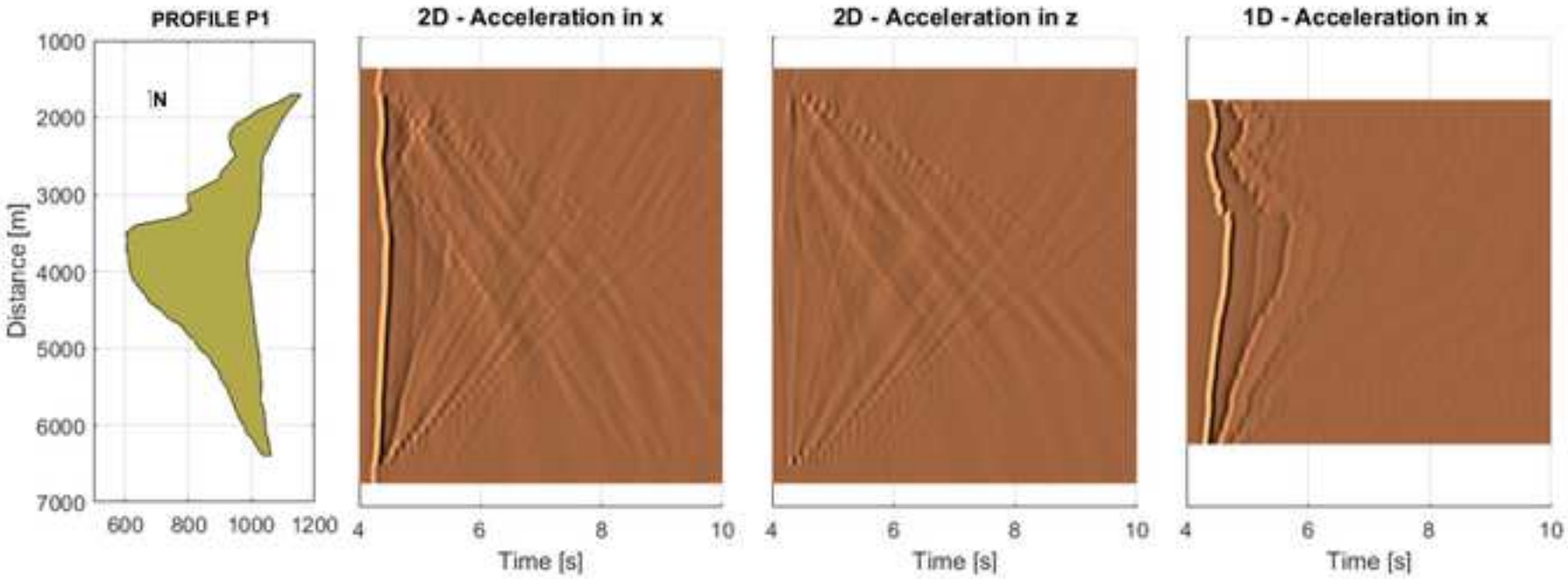

Figure8

Click here to download Figure Figure8.jpg

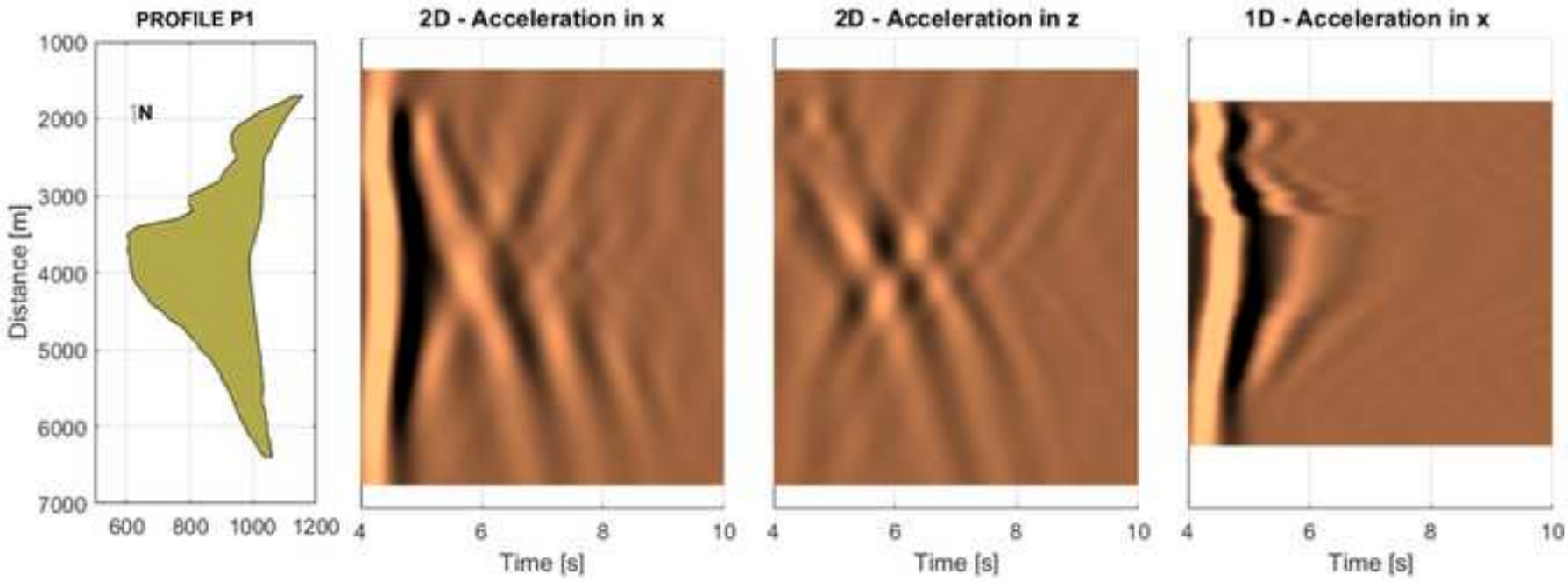

Figure9

Click here to download Figure Figure9.jpg

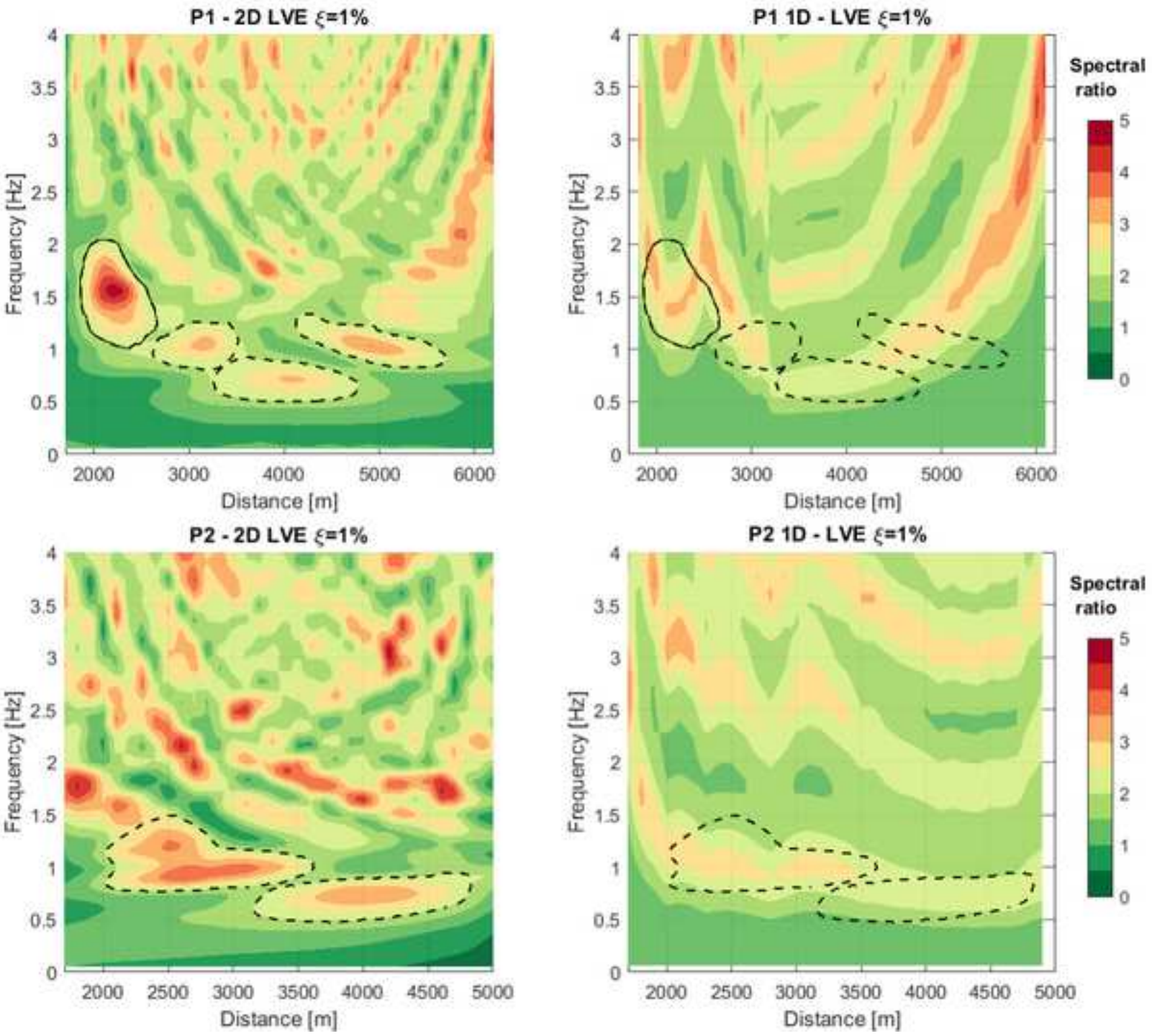

Figure10

Click here to download Figure Figure10.jpg

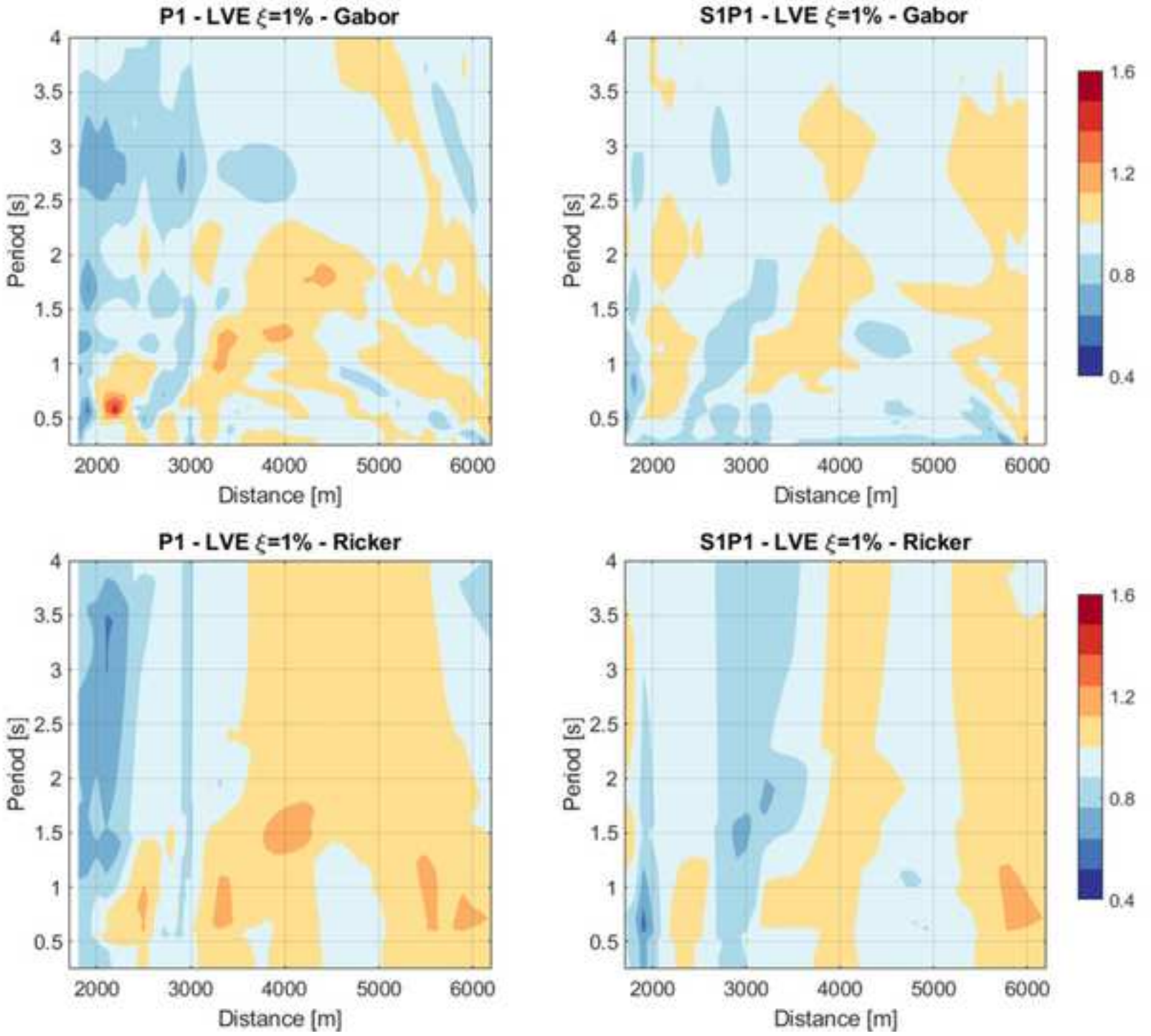

Figure11

Click here to download Figure Figure11.jpg

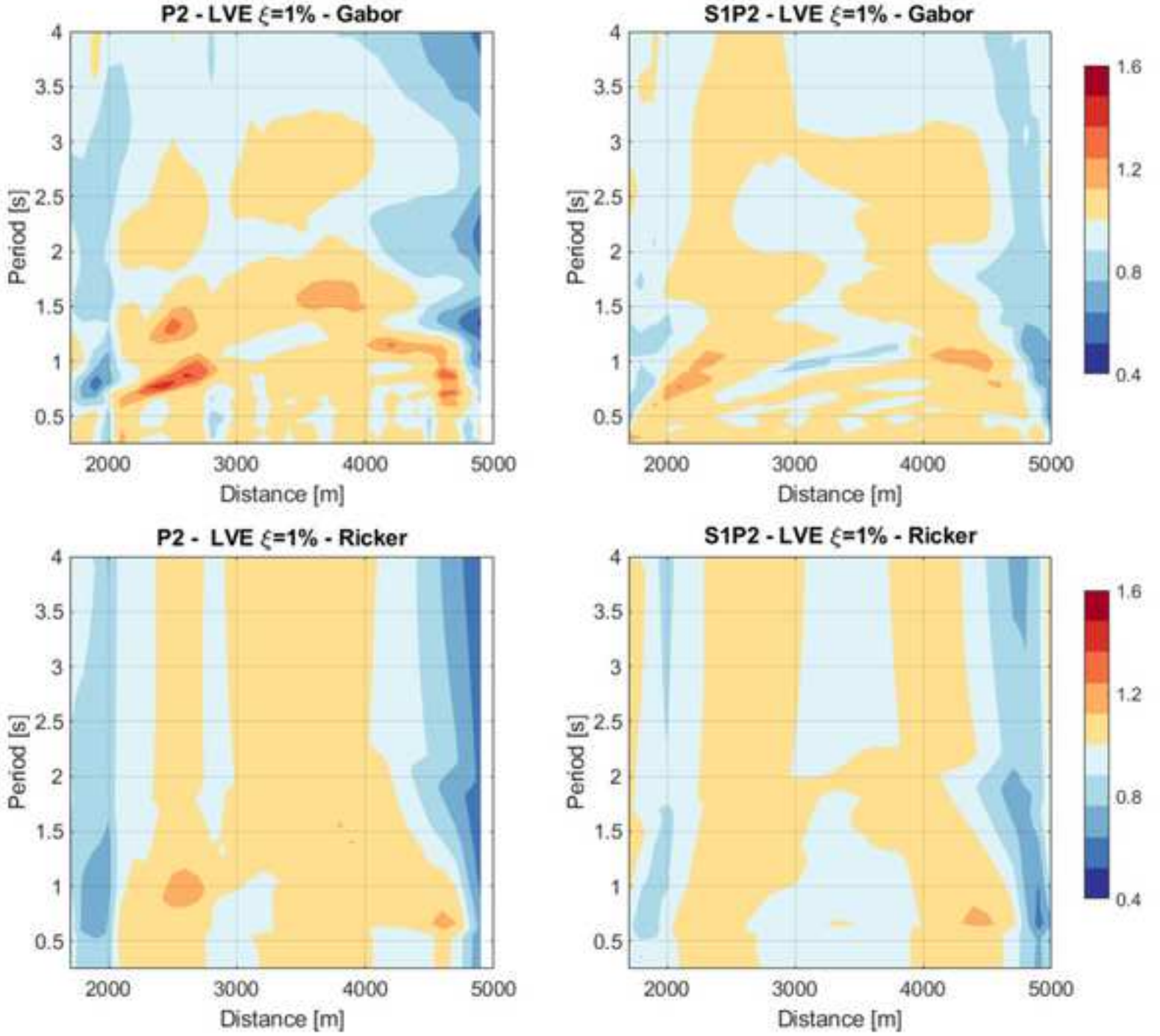

Figure12

Click here to download Figure Figure12.jpg

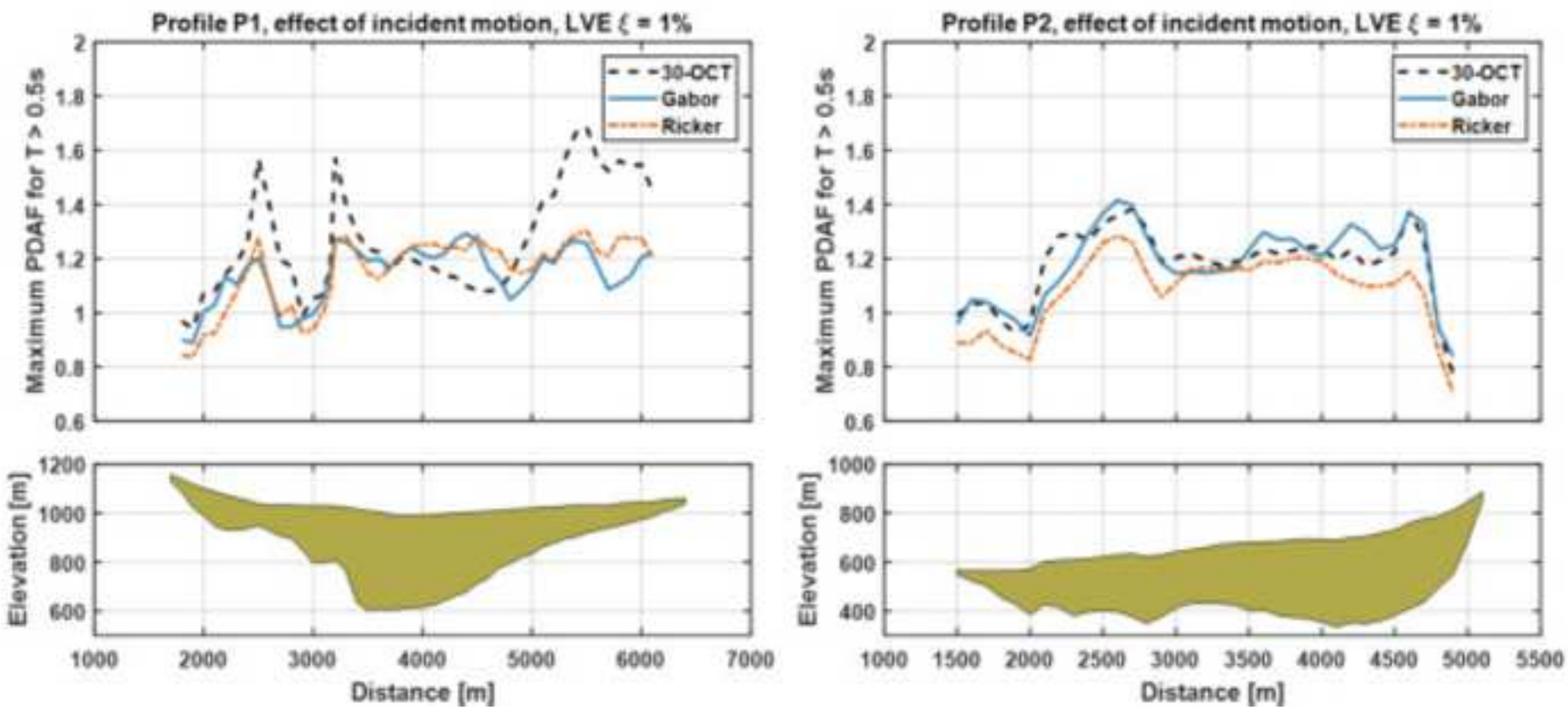

Figure13

Click here to download Figure Figure13.jpg

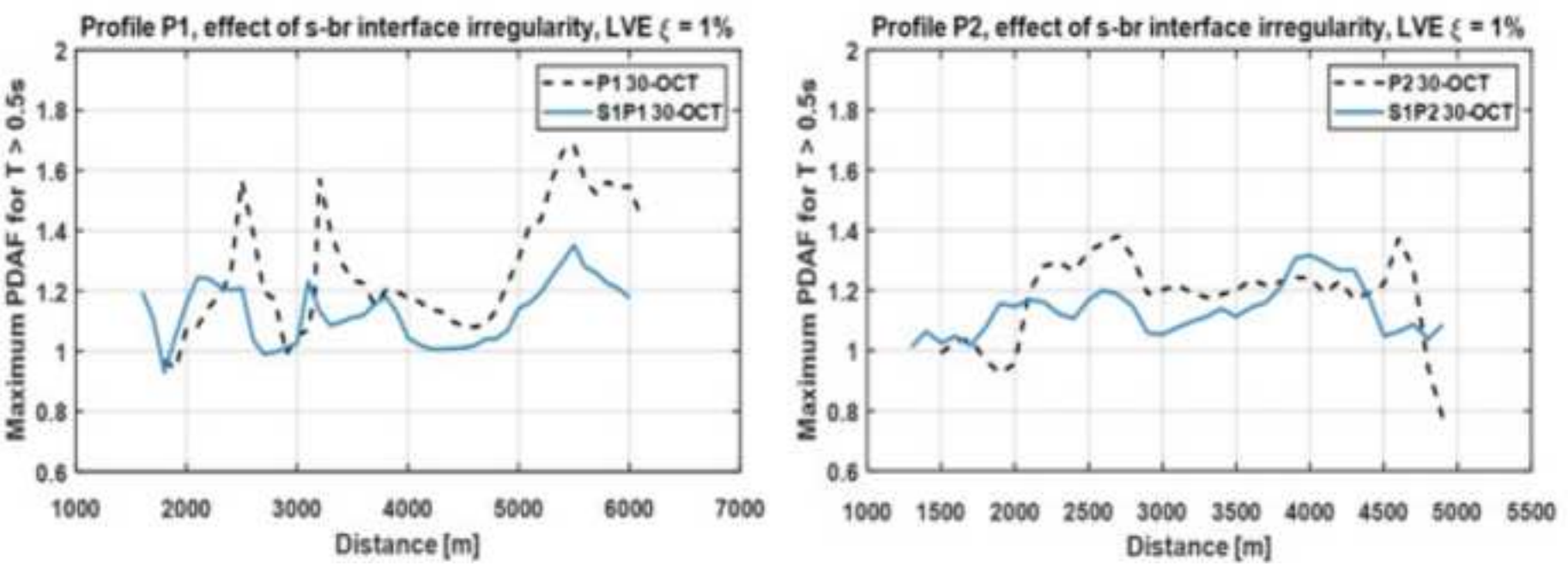

Figure14

Click here to download Figure Figure14.jpg

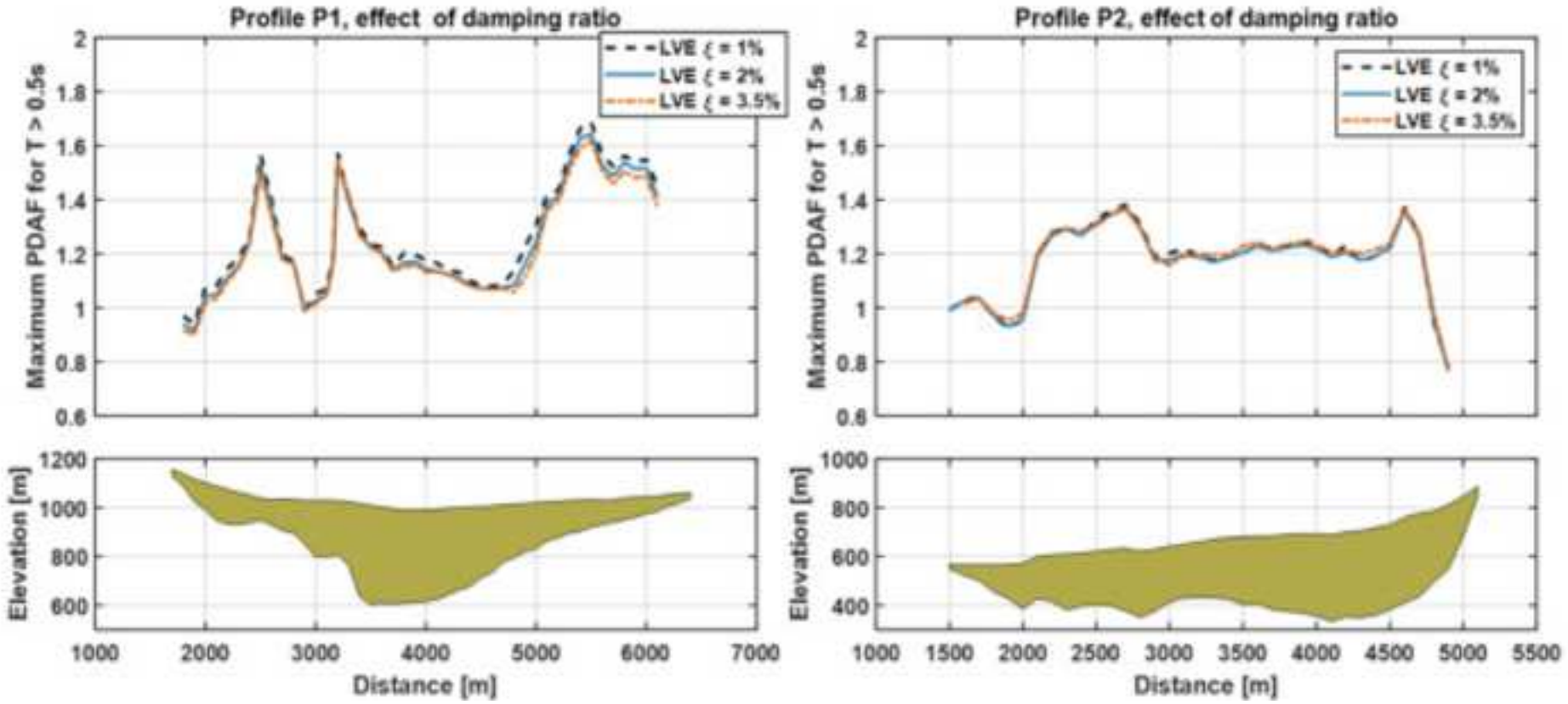

Figure15

Click here to download Figure Figure15.jpg

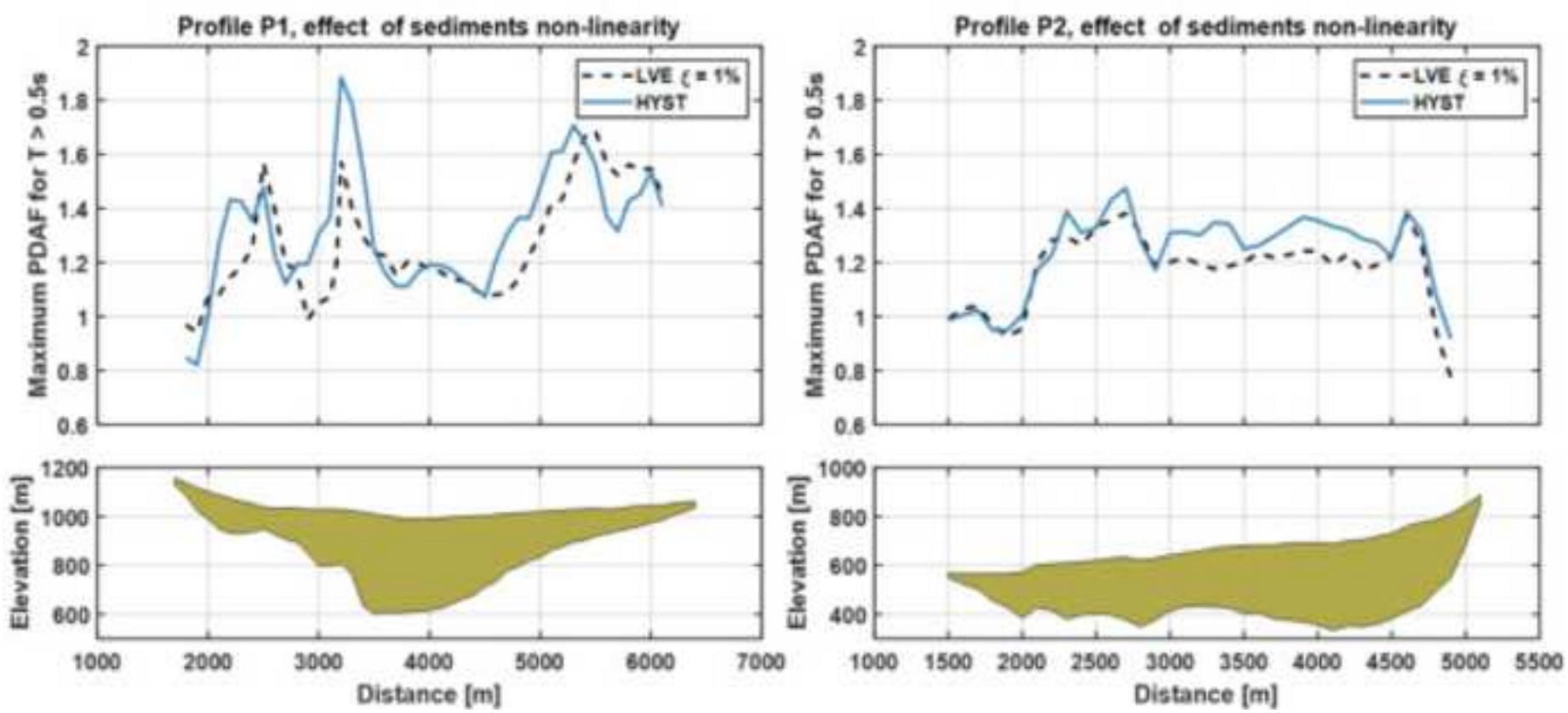

Table2

Click here to access/download

Table

Table2.xlsx

Table1

Click here to access/download

Table

Table1.xlsx

Declaration of interests

☒ The authors declare that they have no known competing financial interests or personal relationships that could have appeared to influence the work reported in this paper.

☐The authors declare the following financial interests/personal relationships which may be considered as potential competing interests: